M.Sc. Hydrology
Department of Earth and Climate
Faculty of Science
Free University Amsterdam

Quantifying the variability of groundwater recharge in the Netherlands with precipitation intensity, landscape properties and season

A time series analysis with nonlinear and nonstationary Impulse Response Functions

submitted by Ellen A. Starke (2777415)
June 28, 2025

— supervisors —
Wouter Berghuijs, Faculty of Science, Department of Earth and Climate
Ype van der Velde, Faculty of Science, Department of Earth and Climate

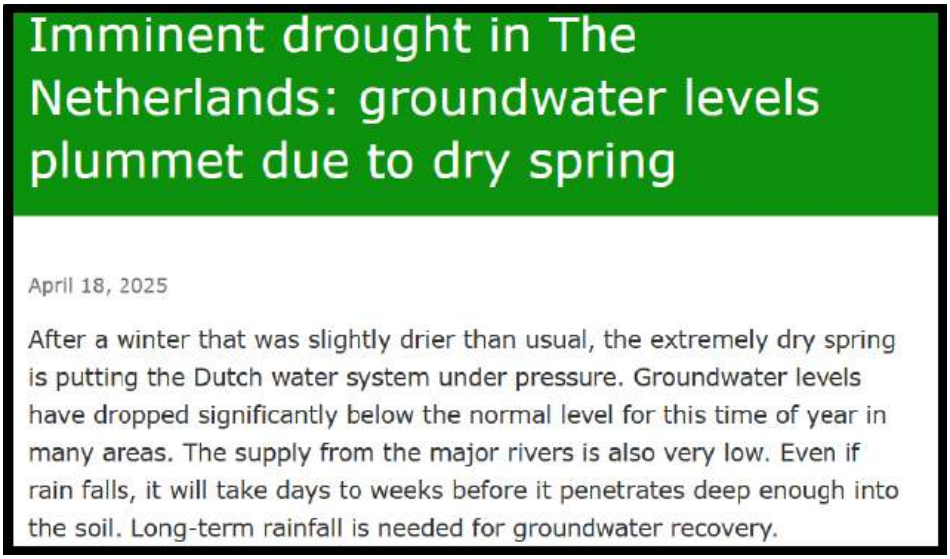

Figure 1: Drought warning issued on 18.04.2025 by Wageningen Environmental Research (2025). Although traditionally a water-rich country, the Netherlands faced water shortages more frequently in recent years. The warning also highlights that rainfall does not immediately relieve groundwater bodies.

Abstract

How groundwater bodies respond to precipitation events can vary with the properties of the precipitation, the aquifer, and ambient, nonstationary conditions. Yet hydrological models often simplify recharge as time-invariant, proportional fractions of rainfall. This study analyzes the time series of 36 shallow Dutch monitoring wells with Ensemble Rainfall-Runoff Analysis (ERRA), a recently developed program that estimates nonlinear, nonstationary Impulse Response Functions (IRFs).

This study investigates *i)* ERRA's capability to derive realistic IRFs of groundwater recharge and precipitation, and quantifies how recharge responses vary with *ii* precipitation intensity, *iii)* landscape parameters, and *iv)* time. *i)* Ensemble-averaged Groundwater Recharge Response Distributions (GRRDs) are estimated with ERRA. *ii)* Nonlinear Response Functions (NRFs) for 7 precipitation ranges are calculated and their trend in total recharge responses compared to power law functions, whose exponent is used as a parameter of linearity. Then *iii)* the integral and shape parameters of the GRRDs are correlated to soil conditions and mean water table depth. *iv)* seasonal GRRDs are calculated and compared by a summer to winter ratio. The assessment of seasonality is further supported by directional statistics.

The analysis finds that *i)* ERRA estimates clear, interpretable GRRDs and NRFs. *ii)* the water table rise increases linearly with precipitation rates in 52.9 % and sublinearly in 38.2 % of the wells. *iii)* Soil type and mean water table depth are weakly or moderately correlated to the response dynamics. However, the water table rise and timing of peak recharge are more variable in clay than in sand. *iv)* The strongest water table rises occur more than a month later than the strongest precipitation in 30 of 36 wells. The ratio of summer to winter recharge is significantly smaller in sandy aquifers compared to those with clay soils.

These results show that shallow Dutch aquifers often behave disproportionally to precipitation and could be better represented by Nonlinear Response Functions than by linear models. The large variability of groundwater recharge in time and space requires further investigation of the effect of ambient conditions. ERRA's potential to separate the influences of inter-correlated parameters was restricted by data availability, but might be a useful tool for further research.

Contents

List of Figures

List of Tables

Terms and acronyms

agg ERRA parameter: aggregation factor

CESAR Cabauw Experimental Site for Atmospheric Research

C$_m$ Mass concentration in directional statistics (equation 20)

dt ERRA parameter: size of time steps ($\neq$ derivative t)

ERRA Ensemble Rainfall-Runoff Analysis

GRRD Groundwater Recharge Response Distribution

H Groundwater head

IRF Impulse Response Function

KNMI Koninklijk Nederlands Meteorologisch Instituut

m ERRA parameter: number of time steps

MAQ Meteorology and Air Quality Group

NaN Not a Number

NAP Normaal Amsterdams Peil

nk ERRA parameter: number of knots in response functions

NRF Nonlinear Response Function

P Precipitation

R Groundwater recharge (equation 1)

r Strength of mass concentration in directional statistics (equation 21)

S_y Specific yield (equation 2)

W Net groundwater discharge (equation 3)

WRIJ Waterschap Rijn en IJssel

WTD Water Table Depth

WTF Water Table Fluctuation

1 Introduction

Groundwater is both a substantial water resource for anthropogenic use and a major influence on the wider environmental system. In the Netherlands, groundwater provides 60% of drinking water (Leerdam et al. 2023) and is vital for secondary use in agriculture and some industries (Teo et al. 2025). In addition to human consumption, aquifers play an important role in the cycling of nutrients and carbon (Griebler, Avramov 2015) and can mitigate the severity of floods (Chang et al. (2019), Kumar, Yazdan (2022)) and droughts (Wendt et al. (2021), Hendriks et al. (2014)). Understanding the processes that control groundwater bodies is therefore essential. The recharge of aquifers is of particular interest for sustainability studies and resource management (Moeck et al. (2020), Levintal et al. (2023), Hund et al. (2018)).

The process that replenishes ('refills') groundwater is called recharge. Groundwater recharge describes water that infiltrates the soil and joins the saturated zone (Moeck et al. 2020). Focused recharge describes localized fast infiltration through preferential flow paths, such as macropores (Cheng et al. 2017). On larger scales, diffuse recharge occurs: water from precipitation and/or irrigation infiltrates the soil surface and passes through the unsaturated zone with matrix flow (Moeck et al. (2020), Scanlon et al. (2002)).

The relevance of groundwater makes it important to understand how recharge varies in time and space. However, this knowledge remains weakly constrained. Globally, recharge is determined mainly by the amount of incoming water, i. e., precipitation and, if occurring, artificial irrigation (Kim, Jackson (2012), Moeck et al. (2020)). Yet the recharge response of the aquifers differs between climate conditions (Barron et al. (2012), Moeck et al. (2020)), vegetation types (Moeck et al. (2020), Kim, Jackson (2012), Huijgevoort et al. (2020), Owuor et al. (2016)), evaporation (Boumis et al. (2022), Moeck et al. (2020)), and water table depth (Smerdon et al. 2008). Even in human-controlled aquifers, spatial heterogeneity can cause significant variability (Moeck et al. 2017).

What fraction of precipitation becomes groundwater recharge depends mainly on the amount of precipitation (Moeck et al. (2020), Kim, Jackson (2012)). For example, recharge responds over-proportionally to extreme precipitation in the tropics and North America (Jasechko, Taylor (2015), Zhang et al. (2016)). In temperate climates, the (non-)linearity of recharge to precipitation appears to depend on the thickness of the unsaturated zone (Zaadnoordijk et al. (2019), Hunt et al. (2008), Doble, Crosbie (2017)). Shallow aquifers are commonly considered linear (Tashie et al. (2016), Zaadnoordijk et al. (2019)). However, a nonlinear model of the unsaturated zone provides a better representation for a shallow aquifer in Austria (Collenteur et al. 2021), so this simplification may not reflect physical processes. In the Netherlands, time series analysis with linear models returns good results except in the deeper aquifers of South Limburg and the Veluwe, yet no other spatial pattern has been identified (Zaadnoordijk et al. 2019). This suggests that there might be other parameters than water table depth that could influence the assumption of linearity.

The recharge of groundwater also varies over time (Jasechko et al. (2014), Jasechko et al. (2017) Moeck et al. (2020), Barron et al. (2012)). Influences on recharge, such as precipitation and vegetation, can be seasonal for themselves, but groundwater recharge shows significant seasonality even when normalized to the amount of rainfall (Jasechko et al. (2014), Tashie et al. (2016)). On a sub-seasonal time scale, the antecedent soil water content has been identified as one dominant factor (Liu et al. (2019), Dripps (2012)). Nonstationarity is even more challenging because some of the influences are inter-dependent. For example, the seasonal variation of air temperatures influences vegetation interception, evaporation rates, and soil moisture content, each of which can affect groundwater recharge (Boumis et al. (2022), Liu et al. (2019), Jasechko et al. (2014)). Thus, nonstationary behavior, together with spatial variability, makes it challenging to quantify the mechanisms of recharge.

One way to quantify the influences on recharge is to estimate an Impulse Response Function (IRF) between recharge and a forcing (or several), such as precipitation (Peterson, Western (2014), Spannenberg et al. (2017), Alsumaiei (2020)). This raises two problems: First, it requires assumptions about the shape of the IRF; second, how does the IRF include nonstationarity? The Python tool Pastas offers a range of pre-defined response functions to the user, among them exponential and gamma functions, to model groundwater recharge from one or more forcings (Collenteur et al. 2019). The PIRFICT model (Predefined IRF In Continuous Time) chooses predefined IRFs based on characteristics of the system under investigation (Asmuth et al. 2002). For the response of groundwater systems to precipitation, it suggests a Pearson type III distribution that considers the subsurface as a number of linear reservoirs. However, a systematic analysis of nonstationary conditions remains difficult.

Recently, a method has been presented that estimates nonlinear and nonstationary Impulse Response Functions for rainfall and runoff. The Ensemble Rainfall-Runoff Analysis (ERRA) uses segmented linear regression to estimate data-based nonlinear response functions (Kirchner 2024). From the Nonlinear Response Functions of all precipitation segments, an ensemble-averaged Groundwater Recharge Response Distribution (GRRD) can be calculated that shows the recharge response over the time since precipitation (lag time). Although developed namely for stream runoff responses, ERRA has been successfully applied to groundwater recharge on the catchment scale (Gao et al. (2025a), Gao et al. (2025b)).

ERRA addresses the challenges of linearity and stationarity simultaneously: first, by deriving the shape of the NRF from the input data directly, and then by allowing the user to create specific NRFs for different precipitation segments. This gives ERRA high flexibility and makes it possible to compare the effect of high and low precipitation intensities. ERRA also creates NRFs for specified conditions, making it easier for the user to quantify the influence of ambient characteristics.

This study applies ERRA to quantify how recharge responds to precipitation in shallow Dutch aquifers. Recharge is estimated from groundwater heads of 36 monitoring wells with the Water Table Fluctuation method. From the time series of recharge and precipitation, ERRA estimates Nonlinear Response Functions and ensemble-averaged Groundwater Recharge Response Distributions. Through statistical comparison of their total responsiveness and shape parameters, this study aims to answer the following questions:

i Is ERRA a suitable tool for groundwater recharge analysis?

ii How (non-)linear are recharge responses to precipitation intensity?

iii How strongly are recharge responses related to landscape characteristics?

iv How strongly do recharge responses vary between summer and winter?

Question *i)* is investigated informally by whether ERRA returns GRRDs with low standard errors (sections 5.1, 5.2). For question *ii)* a power law function is fitted and its exponent is used as a parameter of linearity (section 5.3). Questions *iii)* and *iv)* apply the Spearman correlation and the Mann-Whitney U test of similarity. In *iii)*, the total response and shape parameters of the GRRDs are related to soil information and the mean water table depth of the aquifers (sections 5.4 and 5.5). Seasonality, *iv)*, is first quantified with directional statistics of the time series. Then ERRA divides the input time series by season, then the ratio of the summer and winter response is statistically evaluated (section 5.6).

2 Theoretical background

This section provides a short overview of the study's wider context. First, it describes the state of groundwater in the Netherlands (2.1), then discusses the Water Table Fluctuation method that is applied to estimate recharge (2.2) and explains how ERRA calculates the Impulse Response Functions that this study uses (2.3).

2.1 Groundwater recharge in the Netherlands

The Netherlands is a country whose annual water input through its large river systems and precipitation exceeds the output (evaporation, discharge) (Royal Netherland Meteorological Institute (KNMI) n.d.). Its subsurface is dominated by a medium-grained sandy soil that is at surface level in the eastern part of the country, but is overlain by semi-confining layers of peat and clay further west, thus, except in some elevated areas in the south and southeast, the groundwater table is close to the surface (De Vries 2007). Where the surface soil is sandy, higher annual water table fluctuations occur, although annual fluctuation remains mostly below 1.5 m (Zaadnoordijk, Lourens 2019). Groundwater in the more elevated sandy areas responds more strongly to precipitation (Zaadnoordijk et al. 2019). Importantly, the response is lower near surface water bodies and in polders (Zaadnoordijk, Lourens 2019).

Despite being a traditionally water-rich country, the Netherlands faces some challenges. Groundwater levels and recharge rates have already been declining since the second half of the twentieth century (Witte et al. (2019), Naeimi (2021)). Water shortages during summer are considered a major threat, especially in the elevated areas of the country (Leerdam et al. (2023), Bense et al. (2023)). In recent years, severe droughts have highlighted concerns about future water availability (Bartholomeus et al. (2023), Thissen et al. (2017)). Since the Netherlands is heavily dependent on groundwater extraction (Leerdam et al. 2023), better knowledge of recharge processes is required.

Groundwater recharge is expected to evolve with ongoing climate change, potentially affecting the quantity and timing of recharge. Climate change is predicted to alter rainfall patterns in the Netherlands. Annual precipitation is expected to increase, but to shift toward winter, increasing the already existing rainfall deficit in the summer months (Bresser et al. (2005), Hurk et al. (2014)). In addition, short, intense precipitation events are likely to occur more frequently (Bresser et al. 2005). This more pronounced seasonality of rainfall is likely to increase the total annual and winter recharge (Engelenburg et al. 2018). Witte et al. (2009) argue that summer recharge may also increase due to dryer soil conditions reducing the fraction of rainfall that evaporates or is taken up by plants. However, the effect on recharge can strongly depend on local characteristics, such as whether the aquifer is connected to surface water or to the root zone of vegetation (Engelenburg et al. 2018). The latter implies that recharge response may vary significantly with (seasonal) water table depth. Quantifying the effect of landscape parameters and seasons thus may support the development toward more resilient management and conservation practices.

2.2 Estimating groundwater recharge with water table fluctuation

Groundwater recharge is defined as a vertical flux that reaches the water table and adds to the aquifer (De Vries, Simmers 2002). It is usually approximated rather than measured directly, and methods are various (Singh et al. (2019), Scanlon et al. (2002)). As a linear and stationary simplification, recharge can be treated as a fraction of precipitation or the missing term in a water balance (De Vries, Simmers (2002), Scanlon et al. (2002), Dingman (2015)). The infiltration process can be followed with tracers (Li et al. (2017), Huang et al. (2019), Moeck et al. (2017)) or models of the unsaturated zone (Gumula-Kawecka et al. (2022), Turkeltaub et al. (2015)). Another approach is to monitor the fluctuations of the groundwater head over time (Becke et al. (2024), Crosbie et al. (2005), Healy, Cook (2002)).

The greatest advantage of this Water Table Fluctuation (WTF) method is its simplicity: It does

not require detailed information about the unsaturated zone (Healy, Cook 2002). Also, groundwater time series are widely available in many parts of the world and can be evaluated at low cost Becke et al. (2024). The performance of recharge estimates by Water Table Fluctuation is considered comparable to water budgets (Labrecque et al. 2020), modeling of the unsaturated zone (Gumula-Kawecka et al. (2022), Jie et al. (2011)), and even products of the GRACE satellite mission (Walczuk et al. 2025). The WTF defines recharge (R) as proportional to the change water table H over time (t) (equation 1). The specific yield S_y represents the relationship between the water table and the volume of the aquifer which depends on the pore space between the soil grains (equation 2).

$$R = S_y * \frac{\mathrm{d}H}{\mathrm{d}t} = S_y * \frac{\Delta H}{\Delta t} \tag{1}$$

$$S_y = \frac{\Delta V_w}{\Delta V_{tot}} = \frac{\Delta V_w}{\Delta H * A} \tag{2}$$

Despite its simple concept, the WTF method comes with some notable challenges (e.g., Freyberg et al. (2015)): First, the specific yield S_y can be difficult to determine. Second, the fluctuation may be the result of other processes other than recharge.

Specific yield S_y (equation 2) is defined as the ratio of the volume of water being drained or added ΔV_W and the change in the total volume of the saturated zone ΔV_{tot}. The latter is often defined as the horizontal area A of the aquifer multiplied by ΔH. Specific yield describes the potential storage volume within the subsurface and is therefore a property of the soils and rocks that form it. Estimating specific yield values is a major cause of uncertainty in recharge investigations (Crosbie et al. 2019). Walker et al. (2019) show that high uncertainties in measuring or estimating S_y propagate into recharge uncertainties with deviations of up to 300 %. Additionally, specific yield varies spatially (Puntu et al. 2023) and with antecedent wetness (Freyberg et al. 2015).

Furthermore, the rise in water table may not be caused by recharge alone. In this case R becomes a net recharge (Becke et al. 2024). The most notable processes that additionally decrease the water table are groundwater discharge and groundwater evapotranspiration (Healy, Cook (2002), Healy (2010), Jie et al. (2011)). Recession rates can be added by quantifying the water table decline between recharging events (Healy, Cook (2002), Healy (2010)). Assuming that they represent net groundwater discharge, recession rates can be extrapolated forward into periods of increasing water table and treated as the baseline from which the water table rises. Thus, equation 1 is adapted to equation 3, with W as a summary term for net discharge and other processes that remove water from the aquifer. Equation 3 is used, for example, by Eaton (2020) and Cuthbert (2010). Mathematically, recession behavior has been described as linear (Cuthbert et al. (2019), Wilopo, Putra (2021)), exponential (Gumula-Kawecka et al. (2022), Delin et al. (2007), Heppner, Nimmo (2005)), power law functions (Heppner, Nimmo (2005)), or as logarithmic or polynomial (Wang et al. 2014). In shallow aquifers recession can be nonstationary due to the seasonality of evapotranspiration (Boumis et al. 2022).

$$R = S_y * \frac{\Delta H}{\Delta t} + W \tag{3}$$

Water table increases can occur as a result of inflow from surface water bodies. In the Netherlands with its extensive drainage systems, this is a particular challenge. The typical small and open ditches are virtually never shown on maps, and information about their hydrological regime is hard to find. This study collects distances between the monitoring wells and the closest surface water body it can identify, but this information could be incomplete.

2.3 Ensemble Rainfall-Runoff Analysis (ERRA)

Because estimating recharge from Water Table Fluctuation makes no assumptions about the relationship between precipitation and recharge, groundwater hydrology often approximates Impulse Response

Functions (IRFs), also known as transfer functions or convolution kernels (Hocking, Kelly (2016), Bakker et al. (2007), Asmuth et al. (2002)). Ensemble Rainfall-Runoff Analysis (ERRA) estimates Nonlinear Response Functions from time series of precipitation and groundwater recharge. Equation 4 illustrates exemplary the role that an Impulse Response Function (IRF) plays between the time series of input x and the output y, with τ representing the lag time.

$$y(t) = \int_0^\infty IRF(\tau) * x(t-\tau)\,\mathrm{d}\tau \tag{4}$$

This study analyzes the Nonlinear Response Functions of precipitation ranges and the ensemble-averaged Groundwater Recharge Response Distributions estimated by ERRA. The mathematical foundations of ERRA are laid out in detail in Kirchner (2022). Examples of their hydrological applications can be found in Kirchner (2024). Kirchner (2025) gives a extensive overview of ERRA's settings. The following paragraphs summarize how ERRA derives Impulse Response Functions.

Equivalent to the IRF in equation 4, ERRA estimates a Groundwater Recharge Response Distribution (GRRD) between the time series of precipitation and recharge. However, because groundwater recharge is not necessarily linear, GRRD is treated as dependent on precipitation rates, as shown in equation 5. There, groundwater recharge at time t is written as$R(t)$, the lag time τ, and the precipitation rate $P_{t-\tau}$. With discrete time steps, this becomes equation 6, (t and τ being replaced by discrete indices j and k).

$$R(t) = \int_{\tau=0}^\infty GRRD(\tau, P(t-\tau)) * P(t-\tau)\,\mathrm{d}\tau \tag{5}$$

$$R_j = \sum_{k=0}^{m} GRRD_k(P_{j-k}) * P_{j-k}\,\Delta t \tag{6}$$

ERRA approaches equation 6 with segmented linear regression. To account for the dependence on rainfall, users can divide the data set into ranges of precipitation intensity. Then, for each range, the response over lag times is broken into lag time segments and estimated linearly within each segment. The result is a continuous, data-based Nonlinear Response Function (NRF) consisting of linear segments. Equation 7 shows that the NRF of a defined precipitation range is the product of GRRD and the precipitation. In equation 8, the complete NRF is approximated as the sum of the nk precipitation segments multiplied with the slopes $\beta'_{l,k}$ of their corresponding broken-stick segment, normalized by Δt. The index l represents the segment.

The connection between recharge R_j and the NRF is drawn in equation 9, which is used to estimate the slopes $\beta'_{l,k}$. Unlike equation 6, it makes recharge dependent on precipitation intensity. The constant α represents systemic biases, whereas ϵ_j describes time-variant residuals. The NRF in equation 8 quantifies the recharge response over lag times for a defined precipitation range. From equation 9, a precipitation-averaged GRRD can be defined (equation 10). Its recharge estimation is given in equation 11.

$$NRF_k(P_{j-k}) = P_{j-k} GRRD_k(P_{j-k}) \tag{7}$$

$$NRF_k(P) \approx \sum_{l=1}^{n_k} \beta'_{l,k} \frac{P'_l}{\Delta t} \tag{8}$$

$$R_j \approx \sum_{k=0}^{m} \sum_{l=1}^{n_k} \beta'_{l,k} P'_{l,j-k} + \alpha + \epsilon_j \tag{9}$$

$$avg.GRRD_k = \frac{\sum_{j=1}^{n-k} NRF_k(P_{j-k})}{\sum_{j=1}^{n-k P_{j-k}}} \Delta t \tag{10}$$

$$R_j \approx \beta_k(P_{j-k}) * P_{j-k} + \alpha + \epsilon_j \tag{11}$$

As this study assesses both NRFs and GRRDs, it is important to distinguish between them. Nonlinear Response Functions describe recharge per time step of precipitation at the mean precipitation rate of their segment. With the input time series in mm/hour, the unit of NRFs is $mm/hour^2$ (mm per hour water table rise per hour of precipitation). By contrast, the ensemble-averaged and precipitation-weighted GRRDs (equation 10) give the user the recharge per time step and per unit of precipitation (mm/hour water table rise per hour and mm/hour of precipitation). Fore specific examples, please see Kirchner (2024).

ERRA provides a wide range of additional settings for the analysis of these NRFs and GRRDs. The parameters specified in this study are described in section 4.2 of the methods.

3 Study sites

This section describes the measurement locations from which precipitation and groundwater head time series are used as input for ERRA. (3.1) discusses the selection criteria. After an overview of the selected sites (3.2), short descriptions of each area and its data contribution are provided (section 3.3).

3.1 Selection criteria

Accross the Netherlands, groundwater observation wells have been selected from multiple data sets. Their locations are shown in figure 2 by yellow and brown markers. A summary of the selected wells is given in table 4 in appendix A. Before introducing each data set in detail (section 3.3), the following paragraphs aim to explain the selection process.

The selected wells provide a) at least 5 years of groundwater observations at b) sub-daily observation frequencies. The 5-year period (a) was chosen to ensure that the data reflect a sufficient number of precipitation events. The sufficiency is tested by setting ERRA to require at least 40 data points per segment (section 4.2). Sub-daily measurements (b) are necessary because the data resolution should not be coarser than the recharge response (Kirchner 2024). As Dutch aquifers lie only a few meters below the surface, a high temporal resolution is required, which limits the number of available wells.

The wells are aligned with precipitation gauges no farther than 10 km away. This distance is within the decorrelation distances found by Leth et al. (2021) for a measurement frequency of 1 hour, which dominates in the selected wells. However, the decorrelation distance is often greater during winter (Leth et al. (2021), De Beek et al. (2011)). Individual distances are listed in table 5. Each well is matched with the closest available precipitation gauge, unless another gauge in a radius of 5 km provides a longer time series.

Boreholes from within 200 m of the well provide soil types (DINOloket 2022). The categories given in table 4 reflect the soil above the deepest measured water table. For more detailed descriptions of soil data, see table 6. In general, clay soil, sometimes combined with fractions of sand and peat, dominates the center and the west of the Netherlands. The soil in the southeast is sandy at all well locations except Azewijn and Laag Keppel, where clay dominates.

Using point data neglects the heterogeneity of the measurement sites. Rainfall and landscape attributes vary spatially and thus can affect infiltration and percolation. However, quantifying localized recharge requires detailed knowledge of each measurement site or complex modeling (De Vries, Simmers (2002), Kishel, Gerla (2002), Cuthbert, Nimmo (2013)). Because this study focuses on regional scales, the monitoring wells are assumed to represent their aquifer. Where multiple tubes are available, two of them are selected randomly.

3.2 Sites overview

The brown and yellow markers in figure 2 illustrate the transition from clay to sand soil. From west to east, the groundwater table becomes shallower and more variable (figure 3). This is consistent with the findings of Zaadnoordijk, Lourens (2019). Likewise, the ground surface in the southeast locations is higher (table 4). No suitable wells have been found in the north and the south of the Netherlands; subsequently, locations with considerably higher surface elevation and deeper water tables are not included.

The three land use categories that cover the largest fraction of a 500 m radius around the well locations are used as land cover description (Wageningen Environmental Research 2024) and listed in table 4. The land use map dates from 2023; changes in land use over time are not considered in this study. With exception of Zeving-1 and Zeving-3, the areas are dominated by natural land covers and agriculture. Greenhouses, a common agricultural feature, suggest that rainfall infiltration might not

be spatially homogeneous.

Information on surface water bodies in the vicinity of the well sites remains incomplete and therefore are not part of the analysis. The distances given in table 4 are manual estimates using a QGIS measurement tool on Open Street Map (OpenStreetMap 2024) and stream network maps of the Rijn-IJssel water administration (Waterschap Rijn end IJssel 2024). However, they are included in this report because the potential interactions between aquifers and surface water bodies are an important limitation to the Water Table Fluctuation method.

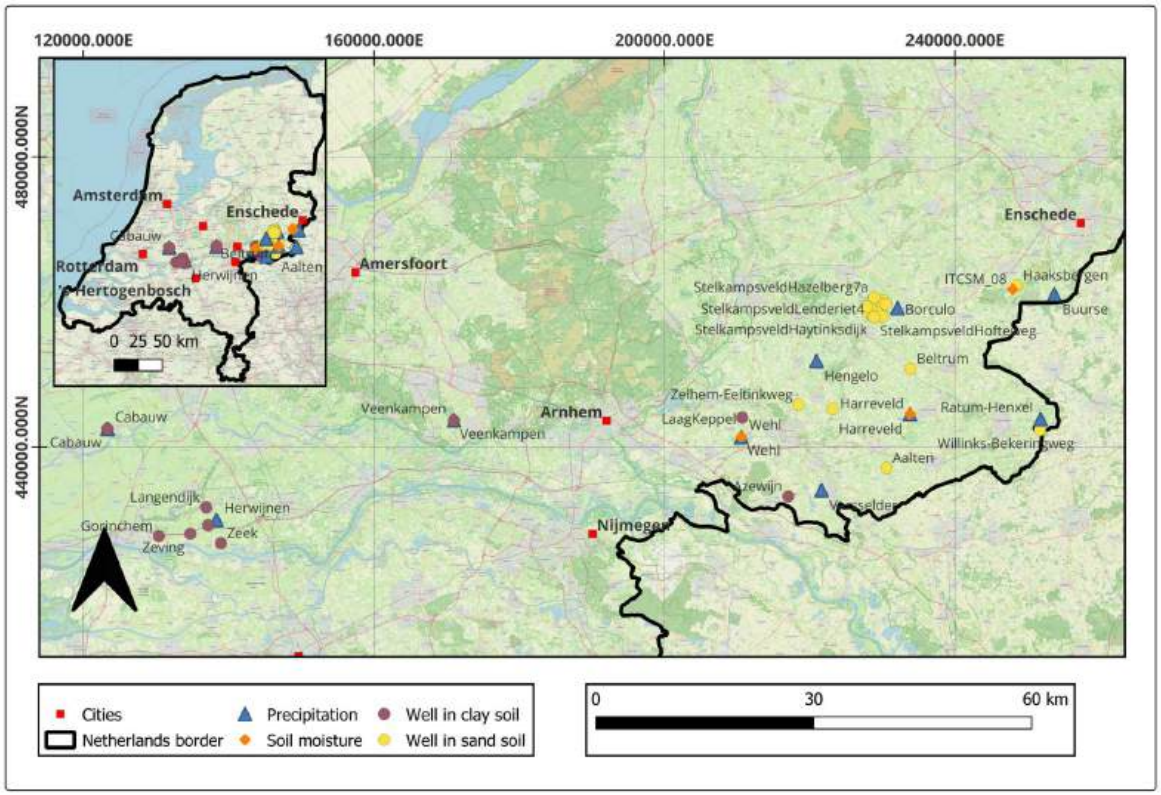

Figure 2: Map of monitoring wells (colored circles) and precipitation gauges (triangles) that are used for Ensemble Rainfall-Runoff Analysis. Surface soil moisture content (orange rhombus) is used to divide seasonal conditions. The wells in the west and center are covered by top layers of clay (brown), in the east the soil is predominantly sandy (yellow).

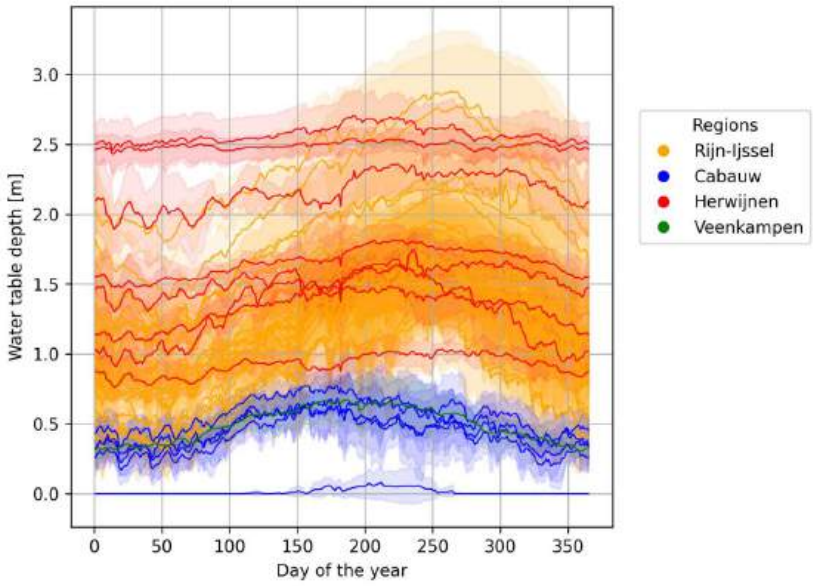

Figure 3: Mean water table depth over day of the year. The shaded areas represent ± 1 standard deviation. The seasonal amplitude of the water table increases from west (Cabauw and Herwijnen, blue and red) to east (Rijn-IJssel, yellow).

3.3 Area descriptions

3.3.1 Cabauw

The Cabauw Experimental Site for Atmospheric Research (CESAR) is located on a polder southeast of Utrecht in the central Netherlands (Ruisdael Observatory 2018a). The site is part of the Ruisdael Observatory and maintained by the Royal Netherlands Meteorological Institute KNMI and other scientific institutions. The surface level of the polder lies about -0.7 m below the NAP. The soil consists of a clay layer of at least 0.7 m thickness, underlain by peat (DINOloket 2022). The polder is characterized by a network of artificial ditches that are designed to maintain the groundwater level suitable for crop growth and peat conservation (Brauer et al. 2014).

GWL4, GWL5, GWL8: the groundwater level is measured with 3 pressure transducers at a frequency of 4 hours and linear gap-filling to a frequency of one hour. These observations cover a period 2003 to 2012 (Wageningen University (2025), Brauer (2014)). The transducers are placed perpendicular to the polder's ditches in a straight line of about 50 meters (Brauer 2014). Less than 200 m away, the KNMI maintains an automatic rain gauge (station ID 348), from which hourly precipitation was obtained. For better alignment, the timestamp of the groundwater observations was rounded to full minutes.

GWLWNN, GWLWNS: also on the CESAR site, groundwater and precipitation are monitored with a frequency of 10 minutes from 2000 to 2024, with the exception of the year 2021 (Royal Netherland Meteorological Institute (KNMI) 2025a). The groundwater level is measured with pressure sensors and calibrated with an accuracy of 2 mm (Bosveld 2020).

3.3.2 Veenkampen

Another location of the Ruisdael Observatory, Veenkampen is maintained by the Meteorology and Air Quality Group (MAQ) of Wageningen University. The location lies 48 km east of Cabauw and 5.7 m

above NAP. The upper soil consists of peat overlain by a clay layer whose thickness gradually increases from zero on the western side to 0.6 m on the eastern side (Ruisdael Observatory 2018b). Land use was converted from farmland to wetland habitat in 2020 (Meteorology and Air Quality Group, University of Wageningen 2018). Although the landscape morphology is similar to Cabauw, the hydrology and water management differ; also the surrounding area also shows a greater variety of soil types (Ruisdael Observatory 2018b).

The groundwater level is measured with a Campbell CS420 submersible pressure transducer and is available at a frequency of 1 minute (Meteorology and Air Quality Group, University of Wageningen 2018). For precipitation, also per minute, an Otto Pluvio S weighing gauge is maintained about 50 m away. The timestamps are evenly spaced, with the well observation having a fraction of 0.01 % and the precipitation data a fraction of 0.60 % NaN. Unrealistically high precipitation values between 2015/07/15 and 2015/08/12 are manually removed from the time series (on the recommendation of the MAQ; these values will not included in later versions of the dataset).

3.3.3 Western Netherlands (Herwijnen)

In the west of the Netherlands, several suitable wells have been identified near the village Herwijnen, north of the Waal River, where the KNMI maintains an automated weather station. The wells record groundwater levels at intervals of three hours; precipitation from the weather station has been resampled accordingly (section 4.1). NaN fractions lie below 1 % for most wells and below 5 % for all. The precipitation time series contains 0.04 % NaN. The sites record groundwater either from 2014 to 2025 or from 2007 to 2020. In all locations, the top soil consists of clay, in case of Zeving sandy clay.

3.3.4 Eastern Netherlands (Rijn and IJssel)

In the east of the Netherlands, the Water administration Rijn and IJssel WRIJ provides hourly time series of monitoring wells. Precipitation is retrieved from the closest rain gauge with hourly observations (table 5). Water Table Depth in all locations lies between 0.5 and 3 m.
The soil type and surface elevation vary within the region. In general, all sites, except for two, have sandy topsoil. The topsoil surrounding the Azewijn well is clay and surrounding the Laag-Keppel well "very sandy" clay (DINOloket 2022).

4 Methods

The theoretical basis of ERRA has already been explained in section 2.3. This section focuses on the practical aspects: the preparation of the time series (4.1), ERRA's parameter settings for the different aspects of the analysis (4.2), and how the ERRA outputs are statistically evaluated (4.3).

4.1 Time series preparation

ERRA is not directly applied to the time series of precipitation and water table depth. First, water table depth must be converted into recharge, which in this study is approximated by water table rise, because estimates of specific yield and long-term recession introduce too high uncertainties (see section 2.2). Lastly, any gaps in the time series are filled with NaN, and the temporal resolution of the impulse and response time series is aligned.

To make the aquifers comparable, the water table depth is used with reference to surface elevation. Surface elevations are taken from DINOloket (2022) where available; for the Cabauw wells GWL4, GWL5 and GWL8 they are provided in the metadata (Brauer 2014), and for GWLWNN and GWLWNS they are kindly supplied by the KNMI. Figure 4 illustrates how the distance between the water table and the ground surface is determined by the elevation of the sensor.

From the water table depth, groundwater recharge is estimated as an increase in the water table. This is analogue to the Water Table Fluctuation (WTF) method (equation 1). However, the specific yield is not included, due to the lack of information and the large uncertainties related to estimations (section 2.2). The Python DataFrame function *.diff()* is used to calculate the difference between consecutive observations (P.andas Community 2008). For the first entry, the water table fluctuation is Not a Number (NaN).

Figure 4: Piezometer sensor at the CESAR observatory, Cabauw. Photograph courtesy of Mariska Konging, KNMI.

Information on specific yield is not available for any measurement location. This limits comparisons between locations. However, recession rates in all locations are low. Periods of zero precipitation for at least 8 days show both declines and increases in the water table. Those with a general reduction in groundwater also contain alternating rise and fall. Fitted linear regression to the 20 longest dry periods in each location retrieves slopes of -1 mm/hour or less with standard errors between 5 and 20 mm. Therefore, recession is neglected throughout this study, as correcting the water table fluctuation

for long-term recession could propagate high uncertainties into the recharge analysis.

One limitation of ERRA is that it requires time series with evenly spaced time steps (Kirchner 2024). To meet this condition, the time series are reassigned to regular time stamps. This way, any times without a measurement value are set to NaN. To ensure that no observations are lost by this procedure, a buffer of 5 minutes is used, and the number of observations is compared between before and after the reassignment.

At the sites in the Herwijnen area (west), precipitation measurements are aggregated to match the measurement frequency of the wells (3 hours). This is done using the Pandas tool *resample('3h').sum()* (P.andas Community 2025). Thus, every value is the sum of the previous 3 hours. If the window contains missing values, the sum is also a NaN to avoid underestimation.

4.2 ERRA settings

This section describes the general function of the ERRA settings used in this analysis. The specific setups dependent on the input data are given in table 1. ERRA settings specific to the type of analysis are given in table 2.

To estimate a general GRRD and its NRFs, at least three parameters are defined: first, the number of time steps m over which they are calculated; second, the number of points (knots) that form the curve nk; third, the length of the timestep dt. The number of time steps m is chosen to cover a period of 48 hours. When specifying the number of points that make up the response functions nk, ERRA distributes them unevenly to represent a range of time scales. The reason is that delayed responses tend to be noisy (Kirchner 2025). As a compromise between accurately representing these late responses on the one hand and eliminating noise on the other, the number of knots nk was set as $m/2$. Lastly, the length of the time step dt is provided. This is an optional parameter that depends on the input data. But, since ERRA returns the recharge responses per time unit, dt helps to compare the results between wells of different measurement frequency. In this analysis, dt is specified to give results with 1 hour as the time unit. The values of m, nk, and dt are shown in table 1.

Additionally, the Veenkampen time series, sampled at a 1 minute frequency, is aggregated with the *agg* parameter that simply gives the aggregation factor. For all other wells, *agg* is 1 by default.

Next, the segmentation of the response functions must be specified. This depends on the kind of analysis for which ERRA is used (see table 2). As the precipitation observed precipitation range varies for all locations, the breakpoints (also called xknots) are not defined by value. Instead, ERRA is set to break the data by even xknots. For most tests, the time series is broken into 6 segments (5 xknots). Only the linearity analysis, where NRF summary parameters are compared between segments, is carried out with 7 xknots. In addition, the minimum number of non-missing values that each segment must contain is specified. This study follows a recommendation by (Kirchner 2025) to use at least 40 non-missing data points per segment. However, this is not possible in the linearity analysis, so there the number is reduced to 30 non-missing values.

For investigating ambient conditions, ERRA can divide the data set by criteria. Based on surface soil moisture content observed in Cabauw and the eastern part of the Netherlands (see figure 2, orange rhombus), the well data are divided into 3 seasonal subsets. Since ERRA requires numerical input, they have been assigned category numbers. First, a 'warm and dry' subset between the 180th and the 300th day of the year got the number 0 (July, August, September, October), a 'cold and wet' subset from the 350th to the 100th day got the number 2 (second half of December, January, February, March), and the transitional phases were assigned the value 1 (April to July, and November and first half of December). In the seasonality analysis in section 5.6, the subsets 0 and 2 are also referred to

as summer and winter.

Table 1: ERRA settings that are specific to the measurement frequency (freq): the number of time steps *m*, the number of curve knots *nk*, the output time step *dt*, and the aggregation factor *agg*.

	Cabauw GWL4-8	Cabauw GWLWNN/S	West	East	Veenkampen	Veenkampen	Veenkampen	Veenkampen	Veenkampen
freq	1 hr.	10 min.	3 hr.	1 hr.	1 min.	1 min.	1 min.	1 min.	1 min.
m	48	288	16	48	288	96	48	36	24
nk	24	144	8	24	144	48	24	18	12
dt	1	(1/6)	3	1	(1/60)	(1/60)	(1/60)	(1/60)	(1/60)
agg	1	1	1	1	10	30	60	90	120

Table 2: ERRA settings that are specific to the analysis. For testing linearity, a higher number of xknots with a lower minimum of non-missing data points is specified.

analysis	xknots	min. number	segments	type
linearity	7	30	8	even
spatial comparison	5	40	6	even
seasonality	5	40	6	even

4.3 Statistical evaluation

For each set of impulse and response time series, ERRA estimates an ensemble-averaged GRRD and one NRF for each precipitation segment. From each of these curves, the following four parameters are derived: first the integral, which represents the total water table response (either per unit of precipitation or per precipitation segment); second the peak height, which is the peak response; third the lag time at which the peak occurs (peak time), and fourth the width of the peak at 50% of the peak height, which represents how dispersed the response is. Those parameters are then compared statistically between the sites.

To quantify relations between these numerical parameters, the Spearman correlation is used, whereas statistical similarity between the soil types of GRRDs or NRFs is calculated with a two-sided Mann-Whitney U test (Mann, Whitney 1947). In Python, this is achieved by the Scipy modules *spearmanr()* and *mananwhitneyu()* (Scipy Community (2008b), Scipy Community (2008c)). The Spearman correlation and the Mann-Whitney U test both are nonparametric and suitable for comparatively small samples.

To compare the GRRDs of multiple stations (i. e., section 5.5), the arithmetical mean $\overline{GRRD}$ and the standard error of the mean $SEM(t)$ are calculated at each lag time. Only lag times represented in at least 50 % of the wells are included in the calculation to avoid bias. Equation 12 gives the mean of the response values $GRRD_i(t)$ for $N(t)$ wells at lag time t. The standard error of the mean se_{mean} is calculated in equation 13.

$$\overline{GRRD} = \frac{1}{N(t)} \sum_{i=1}^{N(t)} GRRD_i(t) \tag{12}$$

$$se_{mean}(t) = \frac{std(t)}{\sqrt{N(t)}} \tag{13}$$

Quantifying the linearity of recharge to precipitation intensity (section 5.3), a power law function is fitted to the integral of the NRF, which represents the total recharge response, against the weighted

mean precipitation of the segment p_{mean}. The power law function (equation 14) is calculated with the Scipy module *curve_fit* (Scipy Community 2008a). Equation 15 shows the standard error of the power law function se_y. The response is considered nonlinear if the exponent n plus/minus one standard error se_n is lower than 0.9 or greater than 1.1. The standard error of n, se_n (equation 16), and the standard error of a, se_a (equation 17), are provided by *curve_fit* (Scipy Community 2008a).

$$\int NRF = y = a * {p_{mean}}^n \tag{14}$$

$$se_y = \sqrt{({p_{mean}}^n * se_a)^2} + (a * {p_{mean}}^n * ln(p_{mean}) * se_n)^2 \tag{15}$$

$$se_n = \sqrt{var(n)} \tag{16}$$

$$se_a = \sqrt{var(a)} \tag{17}$$

Of course, the boundaries for linearity are arbitrary. However, the purpose of the power law fit is not to define such boundaries, but to assess whether the relationship between the recharge response and precipitation intensity is represented best by a linear fit. For comparison, curve_fit is also used to calculate a linear regression that is forced through the point of origin. This condition is made because intercepts would not represent physical boundary conditions: at zero precipitation, no recharge response should occur. The linear fit and its standard error are given in the equations 18 and 19. m is the number of $xknots$, which in the linearity analysis is 7 (see section 4.2). To further assess which fit is a better representation, differences in their coefficient of determination R^2 and Root Mean Square Error $RMSE$ are used.

$$y = b * x \tag{18}$$

$$se_y = \sqrt{\frac{1}{m-1} * \frac{\sum (y_i - b * x_i)^2}{\sum x_i^2}} \tag{19}$$

Seasonality (section 5.6) is further analyzed using directional statistics as suggested by (Berghuijs et al. 2025). The center of mass is calculated as a fraction of the water year (equation 20) and represents the time during which the flux $Q(t)$ is most expressive. It depends on the cosine $\bar{y}$ and the sine $\bar{x}$ of $Q(t)$ (22. The parameter R (equation 21) describes the strength of the center of mass.

$$C_m = \frac{\text{atan2}(\bar{y}, \bar{x})}{2\pi} \tag{20}$$

$$r = \sqrt{\bar{x}^2 + \bar{y}^2} \tag{21}$$

$$\bar{x} = \frac{1}{\int_{t=0}^{t=1} Q(t)\,\mathrm{d}t} \int_{t=0}^{t=1} (\cos(2\pi t)\, Q(t)\,\mathrm{d}t \tag{22}$$

$$\bar{y} = \frac{1}{\int_{t=0}^{t=1} Q(t)\,\mathrm{d}t} \int_{t=0}^{t=1} (\sin(2\pi t)\, Q(t)\,\mathrm{d}t$$

5 Results

Here, the main findings of the study are presented. 5.1 shows example GRRDs and discusses their sensitivity to aggregation in the example of the Veenkampen well. Then, properties of GRRDs and their relationships with each other are discussed (5.2). In 5.3, the relations between the total recharge response of the NRFs and the precipitation intensity are fitted to a power law and a linear curve. 5.4 compares the influence of the landscape parameters soil type and mean water table depth on the recharge responses of the GRRDs. The spatial heterogeneity is further illustrated by the 13 Stelkampsveld wells, which cover a comparatively small area.(5.5). In 5.6, GRRDs for summer and winter periods are compared.

5.1 Recharge distributions: examples and the effect of aggregation

For most of the 36 wells, the Groundwater Recharge Response Distributions show clear peaks and subsequent declines in the recharge response over lag time. This demonstrates that ERRA is capable of capturing groundwater responses, even for fast-responding shallow aquifers. Figure 5 shows examples of GRRDs that show distinct distributions of the water table rise per precipitation. Each GRRD is represents a precipitation-weighted ensemble-average of all recharge responses in the time series. The unit of the response is $hour^{-1}$, which means $mm/hour$ of rise in water table per mm of precipitation.

Figure 5 shows that with lag time, the water table rise initially increases, then peaks, and subsequently decreases again. In most wells, the decreasing phase (or 'tail') is less steep than the increase. The examples vary in the height, width, and also in the timing of the peaks. These shape properties are further discussed in section 5.2. Despite being chosen from different regions, the GRRDs are not representative (see section 5.5 for examples of local variability).

In some wells, the response at the first time step is already close to the peak. In two wells the GRRD peaks at the first time step directly and only shows decline. This is shown in figure 6. At the first time step, the GRRDs of Willinks-Bekeringweg (blue) and Zelhem-Jolinkdijk (orange) have already reached (and possibly passed) their peak response. At the GRRDs of Zelhem-Eeltinkweg (green), Laag Keppel (red), and Haaksbergen (purple), the recharge response at the first time step is already more than 80% of the peak response.

This could indicate a fast initial response that the time series might be too coarse to capture. However, a too fine temporal resolution is problematic, too. The standard error does not decrease proportionally and may even increase. Such a high signal-to-noise ratio is illustrated in figure 7. Originally, the Veenkampen well was sampled at a 1 minute frequency. In this figure, the GRRDs of Veenkampen are shown for different aggregation factors (see table 1). The smallest aggregation to 10 minutes (orange) results in a much noisier GRRD than aggregation to 60 (green) or 120 minutes (blue). Note that the response in the first time step decreases with stronger aggregation. The effect of aggregation on shape parameters will be discussed further in the next section. In every other analysis of the Veenkampen site, the aggregation factor of 60 minutes is used.

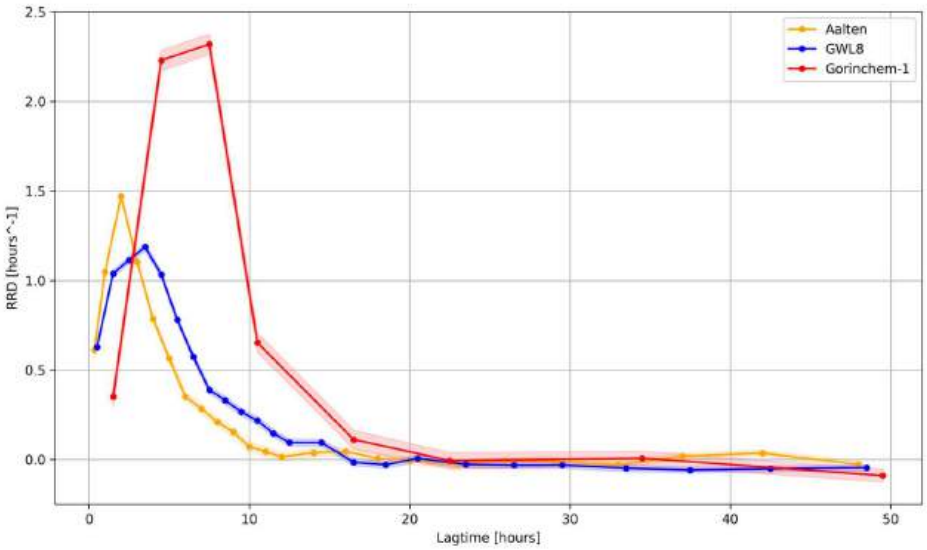

Figure 5: Examples of distinct ERRA-derived GRRDs. These examples all show a clear increase and decline of the water table rise per amount of precipitation with lag time. The shaded area signifies ± 1 standard error.

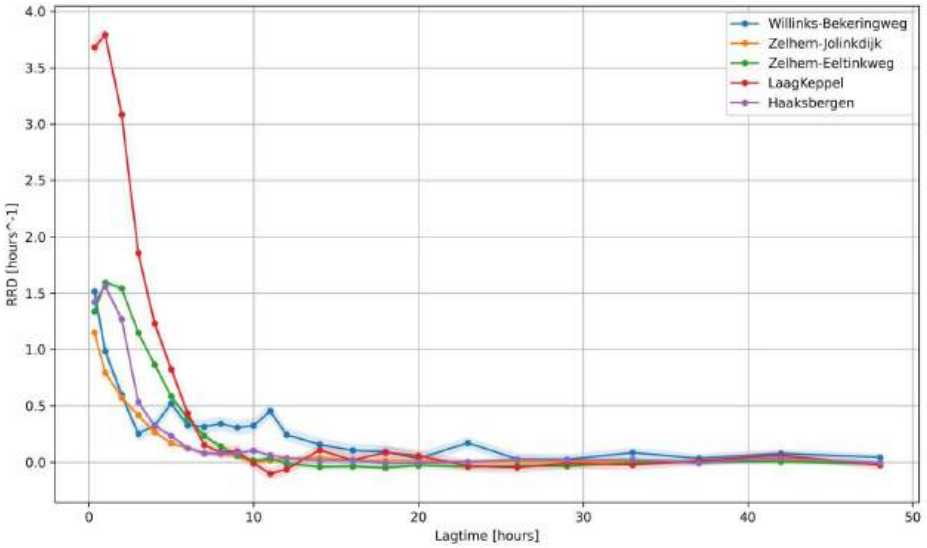

Figure 6: Examples of GRRDs, where the first time step is already > 80% of the peak of the peak of the distribution, indicating that the initial response has not been captured by the time series. The shaded areas represent ± 1 standard error.

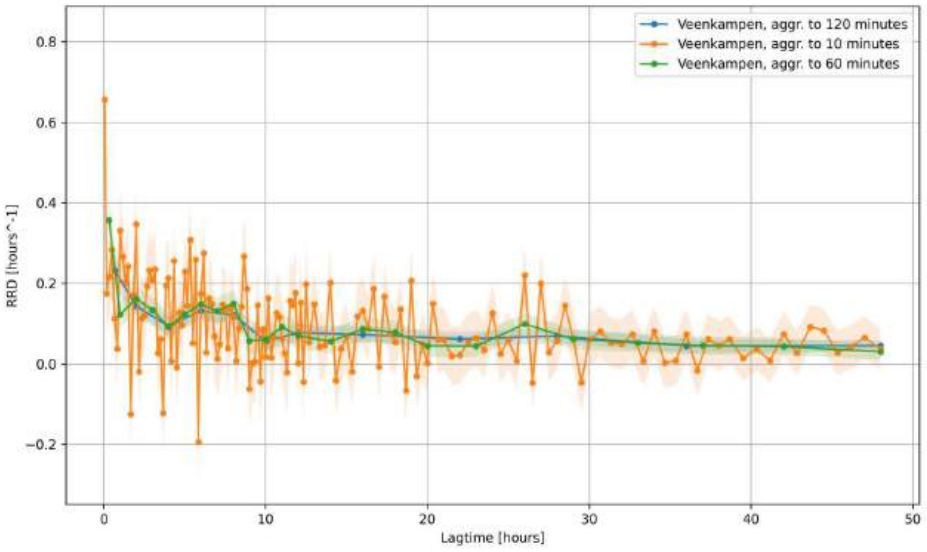

Figure 7: High signal-to-noise ratio in Veenkampen GRRD at fine temporal resolution. With aggregation of the time series from 10 to 60, and 120 minutes, the noise decreases. The shaded areas represent ± 1 standard error.

5.2 Relationships between GRRD properties

GRRDs can be summarized by their shape parameters. ERRA calculates the lag time and height of the peak response, the peak width at 50% of the decline, and the integral of the GRRD. The integral of a GRRD approximates the total recharge response water table rise, that is, the total ensemble-averaged increase in the water table per unit of precipitation. Multiplied by the specific yield, it would equal the recharge coefficient. (Note that the total recharge response is unitless: $hour^{-1} * hour$). This section compares the shape parameters and integral of GRRDs between all wells and discusses how they are related to each other.

Correlations between these GRRD properties show that most of them have strong relations between the total recharge response and the peak height (Spearman $\rho = 0.763$, p = $1.05*10^{-8}$). In contrast, total recharge is not significantly correlated to peak width ($\rho = 0.074$, p = 0.649) or the lag time of the peak ($\rho = 0.234$, p = 0.147). This suggests that, though the water table rise occurs over several hours, the peak response is the most important phase of the GRRD. As the peak lag time can represent the mean travel time of the precipitation through the unsaturated zone, its low correlation with the total recharge indicates that percolation has little effect on the amount of recharge.

However, there is also a strong correlation between peak lag time and peak width ($\rho = 0.860$, p = $1.16 * 10^{-12}$). This shows that both peak width and peak lag time might be indicators of how strongly the precipitation impulse is dispersed in the processes of infiltration and percolation.

Although the peak recharge responses occur over wide ranges of lag time, peak height, and peak width, their distribution is skewed positively. Figure 8 shows the peak response by height and timing, with the marker size and color symbolizing the peak width. All except three wells peak in less than 7 hours of lag time; the median peak lag time is 1.35 hours. The peak responses range from 0.5 ± 0.04 (Zeving-1) to 28.1 ± 3.4 hours−1 (GWLWNN and GWLWNS at Cabauw); but the median peak response is 1.45 $hours^{-1}$, and 80% of the wells have peak responses of less than 3 hours−1, indicating that GWLWNN and GWLWNS might be outliers. (Note that this measure only considers water table

rise without correcting for the specific yield.) The peak widths range from 6.0 ± 1.7 minutes to 15.49 ± 1.87 hours.

Aggregation has has considerable effect on the GRRDs' shape parameters. For Veenkampen, the peak lag time and peak width increase with aggregation, whereas the peak height decreases. This is shown in the bottom plot of figure 8. The markers represent different aggregations of the time series that originally had a resolution of 1 minute and have been aggregated in ERRA to 10, 30, 60, 90, and 120 minutes. Between aggregation of the factor 10 and 120 minutes, the peak lag time increases 12.6 times, which is roughly proportional to the aggregation. The peak width increases by factor 43.8 and the peak height is reduced by two thirds. Thus, the effect on peak height and width of GRRDs may not always be proportional to the aggregation factor. This implies that the relations with shape parameters of other sites may also vary with aggregation.

However, the total recharge response, represented by the integral of the GRRD, appears unaffected by aggregation. For Veenkampen, the mean of all aggregations is 3.58 with a standard deviation of 0.15 (unitless). Thus, the total recharge response is the most reliable parameter for comparisons across time series with different measurement frequencies or aggregation levels.

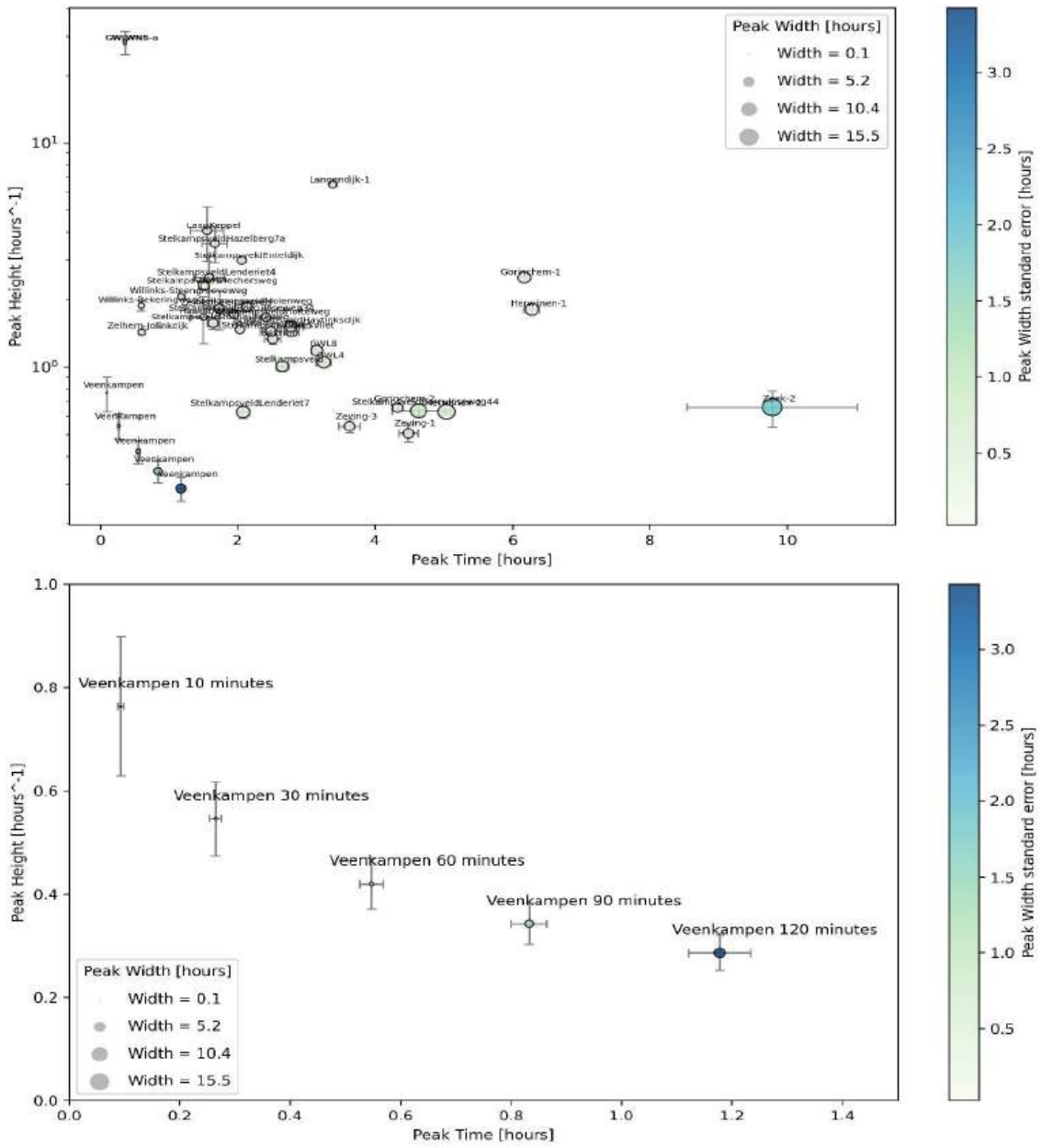

Figure 8: **Top**: Peaks of precipitation-weighted Groundwater Recharge Response Distribution. Peak height as y-axis (logarithmic!), and peak time as x-axis, with error bars signifying ± 1 standard error. The marker size symbolizes the peak width, the marker color the standard error of the peak width. **Bottom**: Close-up to Veenkampen well, aggregated to 10, 30, 60, 90, and 120 minutes. Peak height decreases with aggregation, peak lag time and peak width increase.

5.3 Linear and sublinear increases in response with precipitation intensity

This section investigates how the total recharge response varies with different intensities of rainfall. The Nonlinear Response Functions (NRF) of recharge are calculated for 7 evenly distributed precipitation intensities with at least 30 non-missing data points in each category (section 4.2). The highest category

of precipitation intensity had to be excluded from the analysis, because in the majority of wells it is supported by a much smaller number of events than the other categories, resulting in comparatively large uncertainties. Power law fits describe the change of the integral of the NRFs with precipitation intensity in all wells but two. Two wells with a the coefficient of determination R^2 smaller than 0.6 are excluded from this analysis (Veenkampen and Willinks Bekeringweg).

For 18 of the included 34 wells, the exponent of the power law fit $n \pm n_{se}$ lies in the range between 0.9 and 1.1. Thus, 52.9% the water table rises approximately proportionately with the intensity of precipitation. Of the other wells, 13 increase less than proportionately (38.2%), indicating that the response to intense precipitation might be buffered and possibly reach a threshold response. Figure 9 shows wells with super-linear (top) and sub-linear (bottom) behavior. The super-linear responses can be fitted to a linear function (y=a*x) with only small differences in the coefficients of determination (Aalten: Δ = -0.051; Azewijn: Δ = -0.035; GWLWNN: Δ = 0.054), indicating that a linear model would represent them similarly well. Of the 13 sublinear wells, only one is similarly well represented by a linear fit (Langendijk, R_{power} = 0.998, ${R_{linear}}^2$=0.956) This shows that assuming linearity may overestimate the total recharge of intense precipitation events in 12 of 34 wells.

Linearity appears appears more strongly related to soil texture than to the thickness of the unsaturated zone In figure 10, the exponent n is plotted by soil type, with linear wells marked by black circles. On average, the exponents of the power law fit are smaller in sand than in clay (Mann-Whitney U test: u= 207 of 320, p=0.138). However, a sublinear increase in the recharge responses is more prevalent in clay soil. Only 3/19 sandy aquifers are sublinear, in contrast to 11/15 clay aquifers. No correlation is found between n and the mean water table depth (ρ = -0.088, p = 0.611) or surface elevation (ρ = 0.140, p = 0.416) of the sites, suggesting that within relatively shallow aquifers the disproportionate response does not become more pronounced with average depth.

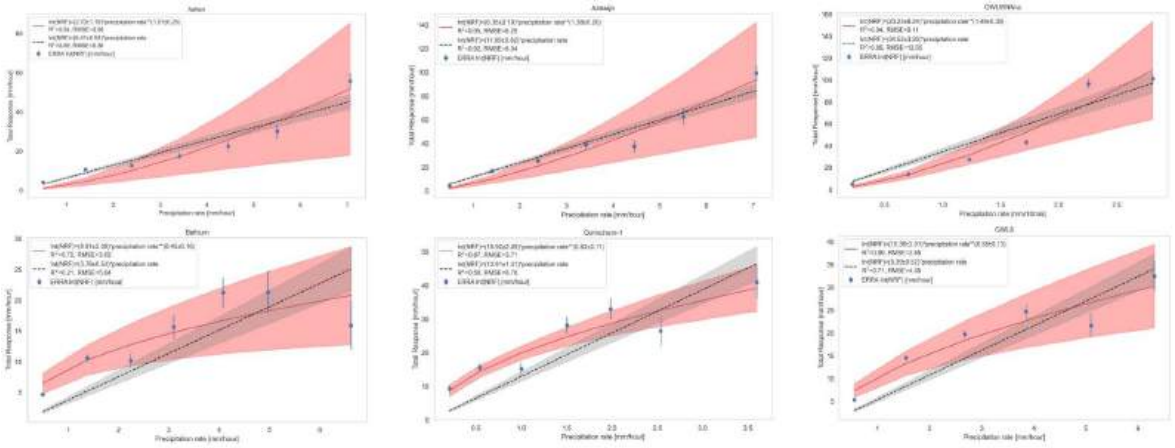

Figure 9: **Top**: Disproportionately high increase in total recharge with precipitation intensity. Note that at GWLWNN (Cabauw), precipitation rates are per 10 minutes. **Bottom**: Examples of less than proportionate increase in total recharge with precipitation rates.

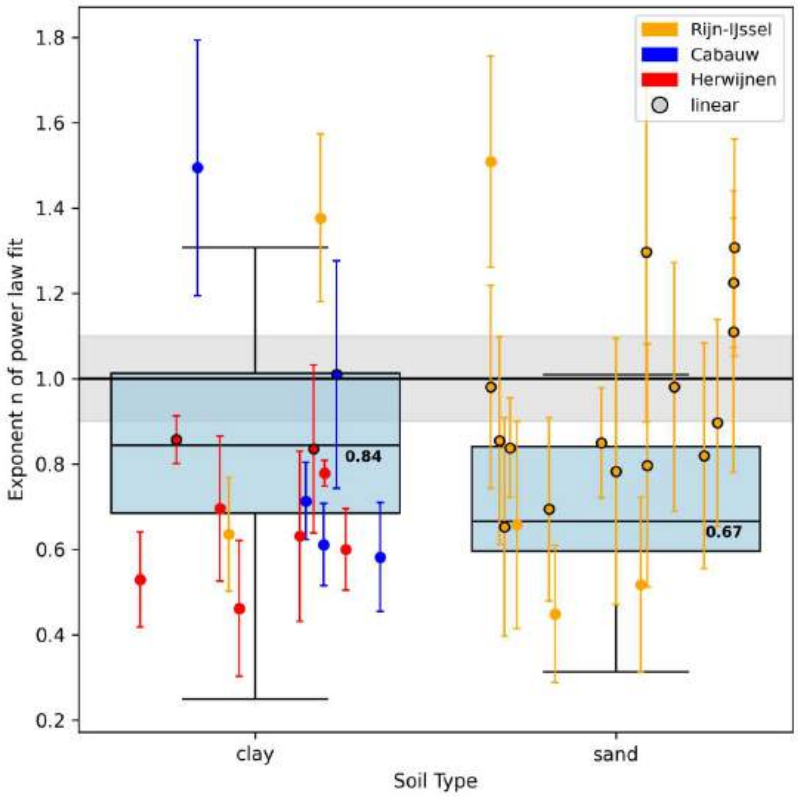

Figure 10: Exponent n of power law fits by soil type. Although the median of the sandy sites is insignificantly lower, the fraction of sublinear exponents is 4.7 times higher in clay sites. The error bars of the markers represents $\pm$ 1 standard error. Markers with a black circle show that the exponent $\pm$ 1 standard error lies within 0.9 and 1.1, and can be considered linear. The whiskers of the box plots represent 1.5 times the inter-quartile range.

5.4 Landscape influences: soil type and mean water table depth

The recharge responses show no distinct patterns for different regions, soil type or mean water table depth (parameters given in table 4). In clay soil, the median total water table rise and the peak lag time are higher than in sands, but the differences are statistically insignificant (Mann-Whitney U test in table 3). Note that this does not consider the any differences in specific yield values. Mean water table depth, given its small range, is moderately correlated to the time and width of the peak response, but not with the total response or the height of the peak response.

Total recharge responses do not differ significantly when the data set is divided into spatial regions, but the peak responses of the Rijn-IJssel region can be distinguished from the other regions. Total and peak responses by region are plotted against peak lag time in figure 11, with the region's median site marked by black circle. Mann-Whitney U tests show that total recharge response, peak width, and peak lag time to do not differ between regions. Responses in the Rijn-IJssel region (yellow) appear less variable than in the other regions, and the peak responses in the Rijn-IJssel area are statistically different from those in other regions ($U = 282$ of 396, $p = 0.023$). The green markers represent different aggregations of the Veenkampen aquifer, see figure 8 for comparison). Overall, geographical proximity is not a reliable predictor of recharge responses.

Neither the total recharge response nor the shapes of the GRRDs differ significantly between soil types (table 3) and figure 12). The median total recharge response is insignificantly higher in clay soil than in sand, but the comparison has limited meaning without specific yield. Also, the median peak lag time is about 80 minutes later than in sand, but this, too, is statistically insignificant (see table 3).

Though not statistically different from sand, clay soils show wider ranges of total recharge responses and peak shapes (table 3, figure 12). The range of total recharge response and peak lag time is about two times larger compared to sandy soils, of peak heights 9.5 times, and of peak width 18.9 times larger. That the shapes of GRRDs vary more strongly in clay soil suggests that recharge is more dispersed there.

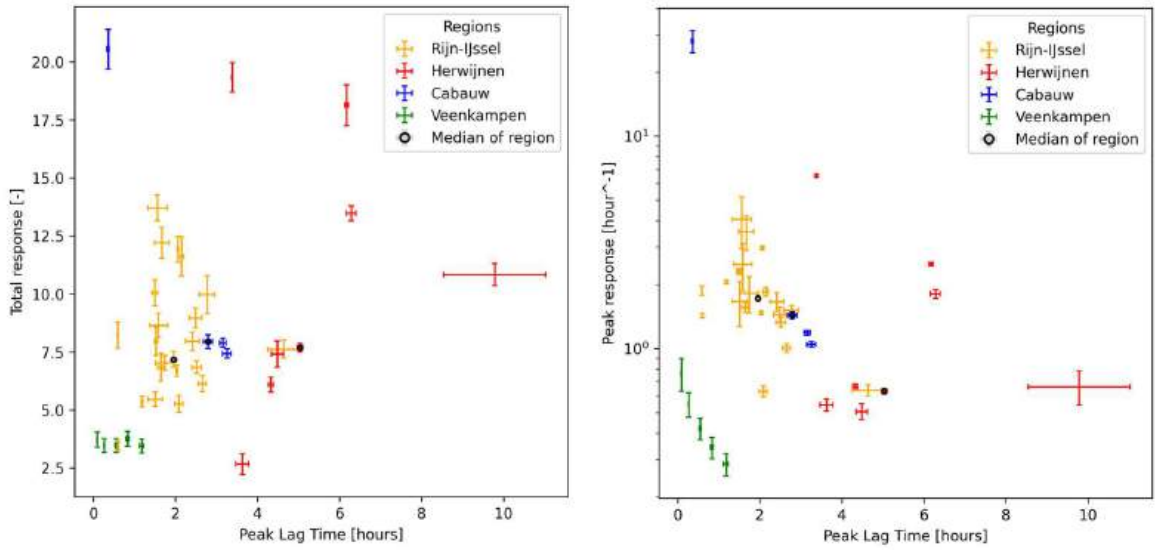

Figure 11: Total recharge response (**left**) and peak response (**right**) versus peak response time, color-coded by geographical region. The y-axis in the right subplot is logarithmic. The error bars signify ± 1 standard error. The median site of each region is highlighted by a black circle.

Table 3: GRRD integral (total water table rise) and shape parameters by soil type: median values and Mann-Whitney U test of statistical significance. Although the median total water table rise and the peak lag time occur later in clay than in sand, this difference is not statistically significant. The U value refers to 320 comparisons.

	clay				sand				Mann-Whitney U	
	med	min	max	range	med	min	max	range	U	p
Total Water Table Rise [-]	9.00	2.67	20.56	17.88	7.40	3.46	12.21	8.75	212	0.101
Peak Lag Time [hours]	3.32	0.36	9.78	9.43	1.99	0.59	4.63	4.04	221	0.054
Peak Recharge [hours^{-1}]	1.31	0.42	28.11	27.69	1.67	0.63	3.56	2.93	142	0.577
Peak Width [hours]	4.65	0.48	15.49	15.02	3.76	1.41	10.21	8.79	191	0.332

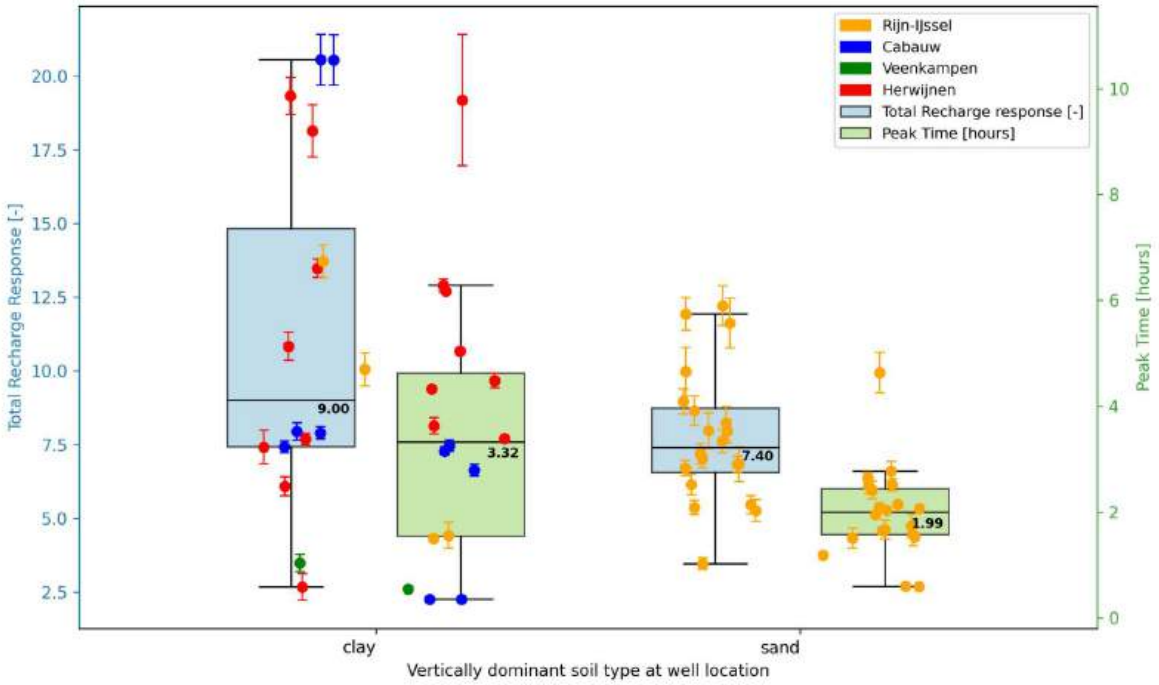

Figure 12: Total recharge response (**blue**) and peak lag time (**green**) by soil type. Though not statistically different, clay (**right**) shows a wider range of responses than sand (**left**). The error bars of the scatter plot represent ± 1 standard error; the whiskers of the box plots represent 1.5 times the inter-quartile range.

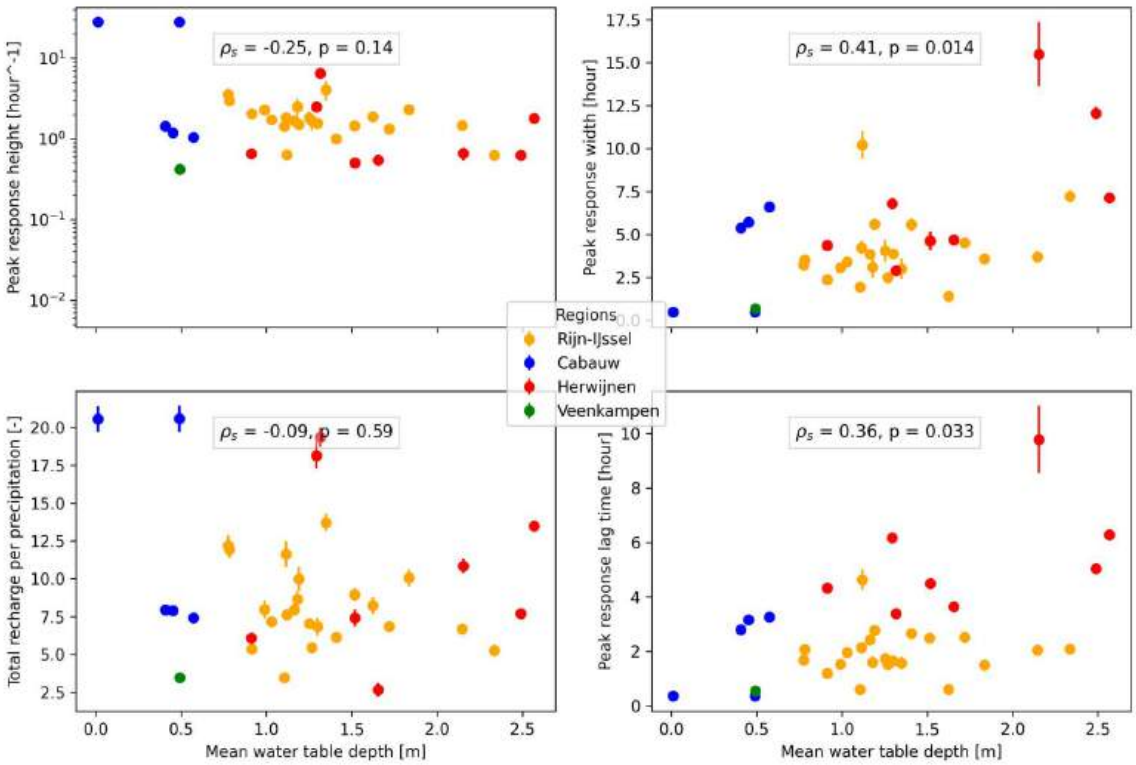

Figure 13: Effect of mean water table depth on peak response (**top left**), peak width (**top right**), total recharge response (**bottom left**), and peak response time (**bottom right**) of GRRDs, color-coded by region. Error bars signify ± 1 standard error. Moderate correlations with the mean water table depth exist for the peak lag times and the peak widths. The peak height and the total response have no strong relation to the mean water table.

There are no strong correlations between the shapes of the GRRDs and the mean water table depth at the sites. Figure 13 shows the peak height, peak width, peak lag time, and total response of all wells plotted against the mean water table depth. Moderate correlations exist with the peak lag time (ρ = 0.620, p = 0.001), and peak width (ρ = 0.454, p = 0.026). This shows that the average path length that precipitation travels through the unsaturated zones influences how strongly the rainfall becomes dispersed, but not how strongly the aquifer responds to precipitation (ρ = 0.007, p = 0.974), nor how pronounced the peak response occurs (ρ = -0.14, p = 0.52).

5.5 Large variability in small areas

Recharge varies not only between landscapes, but also on small spatial scales. To investigate this variability, this section compares the GRRDs of 13 wells in Stelkampsveld, a 3x3 km area in the Rijn-IJssel region. Stelkampsveld is a protected nature area west of Borculo in the eastern Netherlands. Its landscape is a heterogeneous mixture of heath, grasslands, ash trees, wetlands, and farmland (Joustra et al. 2017). Stelkampsveld is part of the Natura 2000 study, which includes endeavors to raise the groundwater level (Joustra et al. 2017).

Figure 14 shows that the GRRDs of the Stelkampsveld wells differ from each other in their recharge

response, their shape, and their peak height. The highest total and peak responses are seen at Enteldijk and Hazelberg 7a. Their total response is more than twice as high as the lowest total response at Lenderiet 7, which also has the widest and one of the lowest peaks. However, Hazelberg 7a is only about 400 m away from Lenderiet 7 and 2.3 km from Enteldijk, showing that their different responses are not the effect of a large-scale landscape change.

Similar small-scale variability can be seen between Borculoseweg 34 (red), which is closest to the arithmetical mean GRRD, and Borculoseweg 44 (light green), the well with the second-lowest peak response. The distance between these wells is approximately 700 m. While their total response is similar (6.85 ± 0.12 and 6.71 ± 0.12), the peak response at Borculoseweg 44 is more than twice as high and three times wider. This illustrates the variability of recharge dynamics, even at small scales and with similar total responses.

Two potential differences between these wells are their subsurface soil and their distance to surface water. 60 m west of Borculoseweg 44 lies an area declared as wetlands that is also surrounded by waterways. This surface water could be connected with the aquifer, and rapid groundwater discharge would cause an underestimation of the recharge response. Also, a borehole west of Borculoseweg 44 (BRO ID: B34D0991) shows half a meter of peat at a depth of 30 cm below ground; although 300 m to the east no peat is found (BRO ID: B34D0993), this shows that the recharge response could be influenced by different soils than Borculoseweg 34 (medium fine to coarse sand). The possible existence of a peak layer might cause precipitation to percolate more slowly than in sand, leading to more dispersed responses to precipitation.

Yet GRRDs still have representative value. Though the examples illustrate that individual GRRDs should not be used as representations of their wider surroundings, they might collectively help to characterize the region. As can be seen in figure 8 in section 5.2, the variability within the Stelkampsveld GRRDs is smaller than the variability within all 36 wells.

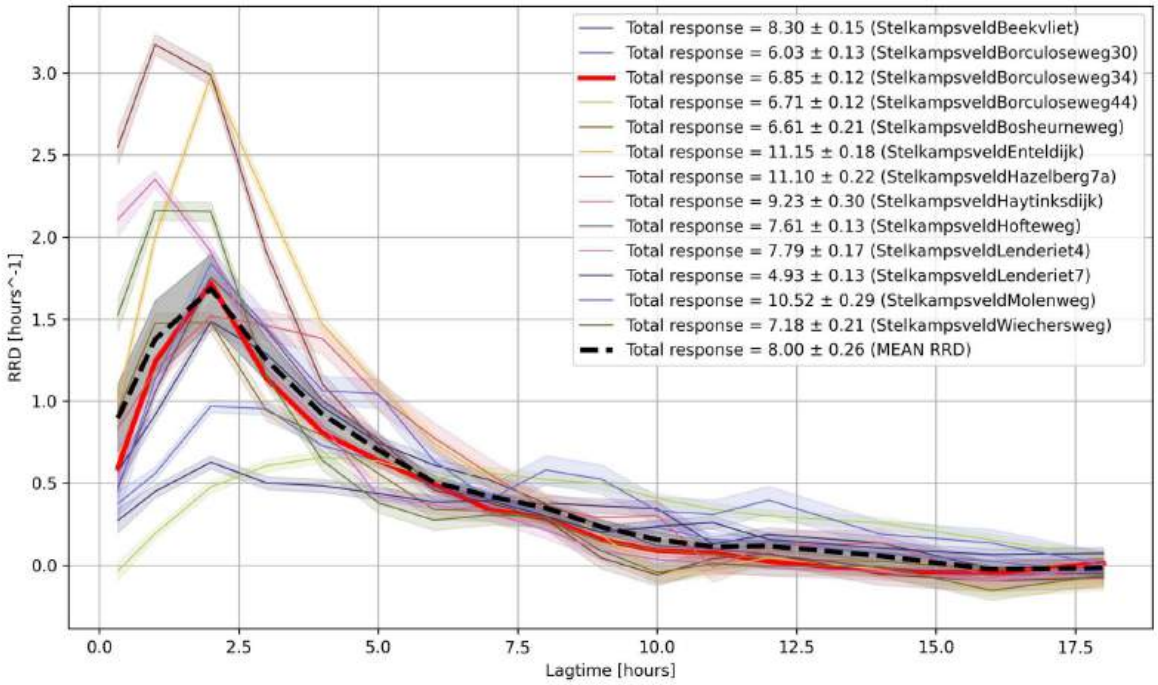

Figure 14: GRRDs from wells of the Stelkampsveld area. Although the maximum distance between them is 2.9 km, the total response and shapes of GRRDs show large variability. The dashed black line represents the calculated mean GRRD. The GRRD that is arithmetically closest to the mean (Borculoseweg 34) is highlighted in red. Shaded areas represent ± 1 standard error.

5.6 Higher recharge responses in winter

This section first analyzes the seasonality of rainfall and recharge with directional statistics, then compares seasonal GRRDs. Note that only 20 sites have long enough time series to enable such a seasonal split, but all sites are used in the directional statistics. The seasonal center of mass C_m of precipitation and the groundwater table of the wells varies across the Netherlands; so does the annual amplitude of the water table. Despite these regional differences, in 30 of 36 wells the center of mass of water table rise occurs more than one month after the center of mass of precipitation. The precipitation time series express only weak seasonal distinctions. For precipitation per week, the highest mass concentration r occurs in Willinks Steengroeveweg (0.18), the smallest in Azewijn (0.028). (This means that 18 and 2.8 % of the rainfall occurred in the wettest average week of the year.) For wells where r is greater than 0.05, the seasonal focus is in November or December in the east and varies from late August to November in the west and center.

Water table depth varies in amplitude and timing across the Netherlands. The amplitudes are higher in the east (1.0 ± 0.21 m) than in the center and west (0.40 ± 0.15 m). The water table is lowest in late summer (June - September) except for some wells in the Herwijnen region (Gorinchem-2, Herwijnen, Zeving-1, Zeek-2) which are deepest in January and February. The wells in the west and center are most shallow at the end of January, and in the east at the end of February / beginning of March.

The arrows in figure 15 A) connect the centers of mass C_m of precipitation (round markers) and water table rise (square markers) for each individual well. In 30 of 36 wells, the center of mass of water table rise is more than a month later. For the east of the Netherlands (Rijn-IJssel region, yellow), water table rise is strongest in January and February; for the other locations, it varies from September

to February. The water table rise in three wells is strongest in summer: Stelkampsveld Wiechersweg, Stelkampsveld Lenderiet 4 (yellow), and Langendijk (red). Possibly, these locations are dominated by events of extreme precipitation. For the others, the the center of mass C_m indicates that the recharge response is strongest at the time of the year when the water table is highest. This suggests that seasonality of the antecedent groundwater level has a greater influence on recharge than seasonality of precipitation.

The center of mass converted to calendar date is shown in subplot B) of figure 15. The center of mass for precipitation (green) corresponds with dates between August and January, whereas for water table rise (brown) it lies mostly in January and February. The strength R of the mass concentration r is similar for precipitation (mean 0.12, standard deviation 0.04) and water table rise (mean 0.14, standard deviation 0.09). At two sites, Willinks Bekeringweg and Stelkampsveld Molenweg, the R is greater than 0.35 indication that their center of mass contains more than a third of their annual water table fluctuation. This result is probably biased by individual large flood events.

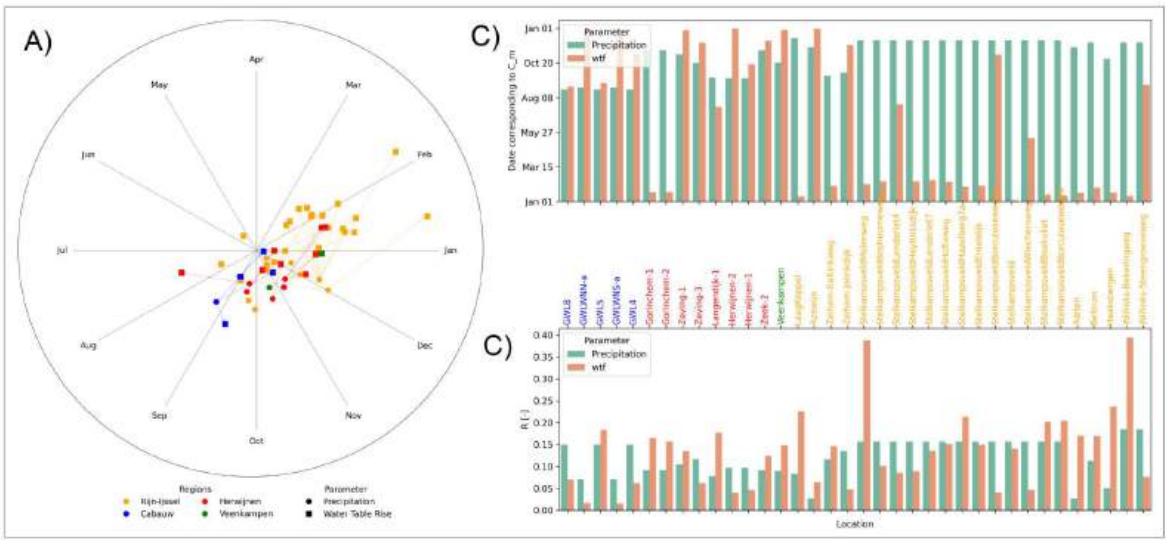

Figure 15: **A**: The seasonal focus of water table rise (square markers) occurs later than of precipitation (round markers). **B**: Center of mass C_m. **C**: Strength of the center of mass r.

The total recharge response differs by season, but the extent of this difference is determined by soil type. Splitting the time series into a summer and a winter season reveals Groundwater Recharge Response Distributions with distinct peak responses for all except three wells. Figure 16 shows the average response in summer divided by the average response in winter, distributed by soil type. The median of the summer response is significantly lower in sand than in clay soils (median(sand) = 0.44, median(clay) = 0.66, Mann-Whitney U test: u=7 of 91, p=0.001. In addition, all wells where no seasonality is observed (summer-winter ratio + 1 standard error greater than 0.9) belong to the clay category. The different recharge responses between soil types can often be explained by the specific yield. However, if the specific yield is assumed to be constant throughout the year, the specific yield should not have an effect on the summer to winter ratio of the responses.

In contrast, the seasonality of the groundwater table shows little influence on the seasonality of the recharge response. The summer-winter ratio is not correlated to the mean water table depth (ρ = -0.162, p=0.496), and moderately correlated with the annual amplitude of the water table depth (ρ = -0.485, p =0.030).

Of the four wells where the GRRDs do not differ significantly with season (circled in black in figure 16), the summer / winter ratio of the GRRD total response is higher than 90% in three: Langendijk, Cabauw GWL5, and Azewijn. In the fourth, Herwijnen-2, the summer average response is 63.3 ± 4.18 % of the winter average response, because the winter response appears to form a second peak that does not occur in the summer response. Herwijnen-1, a different tube at the same location, returns only one peak response phase in all seasons.

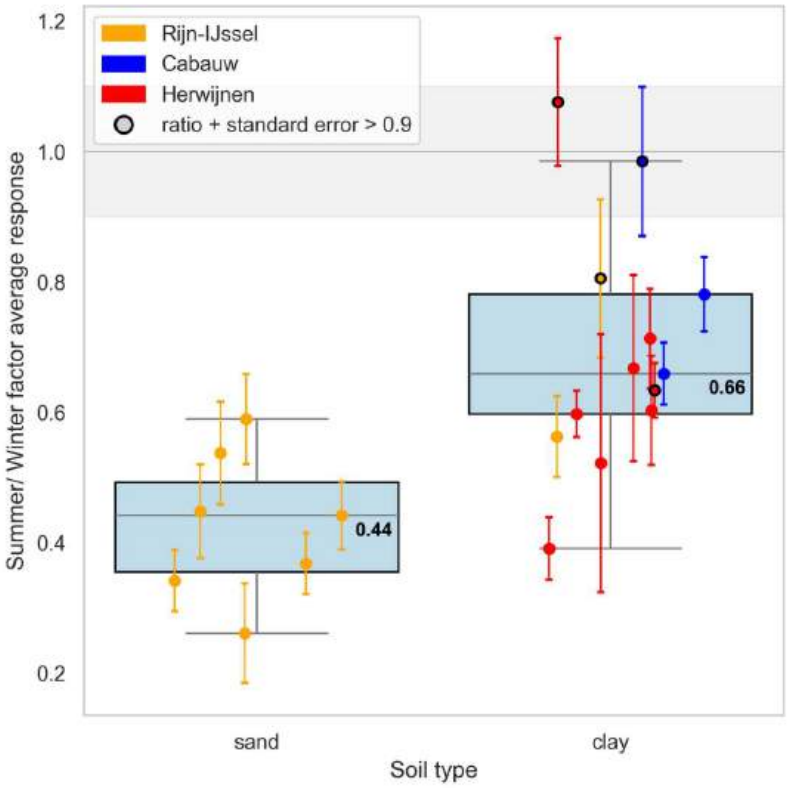

Figure 16: Summer to winter ratios of total response by soil type. The error bars represent ± 1 standard error. Where the ratio + 1 standard error is greater than 0.9, the wells are assumed non-seasonal (marked with a black circle). The median of summer recharge responses is significantly lower in sandy soils compared to clay soils (p=0.001). The whiskers of the box plots represent 1.5 times the inter-quartile range.

6 Discussion

This section refers again to the research questions of this study and discusses how the findings contribute to their answers. 6.1: Is ERRA a suitable tool for groundwater recharge analysis? 6.2: How (non-)linear are recharge responses to precipitation intensity? 6.3: How strongly are recharge responses related to landscape characteristics? 6.4: How strongly do recharge responses vary between summer and winter? The findings are compared with existing literature, highlighting opportunities for expansion of the analysis.

6.1 Is ERRA a suitable tool for groundwater recharge analysis?

ERRA returned clear, interpretable GRRDs and NRFs for most wells (overview in appendix C). GRRDs with low signal-to-noise ratios such as Veenkampen can be smoothed by aggregation (see figure 7 in section 5.1) or by reducing the number of xknots (Kirchner (2025) and section 4.2).

Overall, ERRA appears suitable for regional comparisons. So far, ERRA applications have focused on catchment studies (Kirchner (2024), Gao et al. (2025b), Gao et al. (2025a), Gorkum (2025)), with one large-scale study and another regional study currently in progress (Eslami et al. (2025), Bollen (2025)). On catchment scale, ERRA-derived GRRDs reflect the observed system dynamics more closely than those simulated by a process-based model (Gao et al. 2025a), showing that data-derived Impulse Response Functions benefit small-scale studies and could also improve the understanding of larger regions.

Aggregating NRFs does not affect the relationships between their shape parameters Kirchner (2024), however, increasing aggregation decreases the precipitation intensities. This could explain why the GRRDs shape parameters appear to be disproportionately affected by aggregation in section 5.1. Users should also be aware that ERRA's internal aggregation algorithm applies a moving average to precipitation time series. For long, low-intensity precipitation events, this could potentially influence the NRFs and thus the precipitation-weighted GRRD.

One step before applying ERRA, suitable input time series are difficult to obtain. In the Netherlands, groundwater is monitored at fine spatial and temporal resolutions, but few sites meet all selection criteria (section 3.1). Frequently, sub-daily observations have been made only in the recent years. Although 5 years of hourly measurements can provide 5 precipitation ranges with at least 40 measurements per range (ERRA settings, section 4.2), they are insufficient for further splitting (i. e., the Stelkampsveld wells). Another limit is the availability of close-by precipitation time series to match the wells in resolution. The KNMI maintains 37 automated weather stations on the Dutch mainland (Royal Netherland Meteorological Institute (KNMI) 2025c), but often in too great distance from suitable wells. Thus, even in the Netherlands, with its extensive network of groundwater observations (DINOloket 2022) and precipitation gauges (Royal Netherland Meteorological Institute (KNMI) 2025c), it is difficult to obtain large numbers of data-driven Impulse Response Functions.

6.2 How (non-)linear is the recharge response to precipitation intensity?

Finding recharge responses that are predominantly linear or sublinear is partially consistent with the existing literature. In shallow Dutch aquifers, acceptance rates for recharge models with linear IRF are above 60 % (Zaadnoordijk et al. 2019). In HYDRUS-1D simulations, linear models perform well in sandy soils up to 150 cm of drainage depth (Vonk 2021). Linear responses in sandy aquifers are also observed in section 5.3. In contrast, Vonk (2021) finds superlinear relationships in clay soils and with thicker unsaturated zones in sandy soils. Although a direct comparison is difficult due to the differences in setup, this contrasts with the observed sublinearity found in this study.

Vonk (2021) attributes the nonlinearity in clay to delayed infiltration (because clay is less permeable than sand (Genuchten 1980)). Similarly, thicker unsaturated zones could increase dispersion (Vonk (2021) and see section 6.3). Although the effect of precipitation intensity on the shape of the

response functions has not been investigated systematically in this study, the ERRA-derived parameters do not support this interpretation. The lag time of the peak response appears to increase only in a small number of locations, but more often it declines or does not show a clear trend (appendix E). Similarly, peak width is observed to increase in some locations and to decrease in others. However, these observations have not been quantified systematically due to time constraints. Doing so could be an interesting extension of this study.

(Non-)linearity matters especially in recharge modeling. Nonlinear relationships between precipitation and groundwater recharge have improved modeling performances in shallow aquifers both with real-world and synthetic time series (Collenteur et al. (2021), Long (2015)). This shows that linearity in shallow aquifers deserves more consideration. Implementing sublinear IRFs might improve the accuracy of recharge predictions. As ERRA has only recently been developed, it has not yet been compared to recharge modeling tools with predefined linear and nonlinear IRFs such as PIRFICT or Pastas.

Sublinear groundwater recharge also affects recharge predictions in the face of climate change. The complexity of recharge models especially affects the predicted response to extreme precipitation (Moeck et al. 2016). The frequency of extreme rainfall events in the Netherlands is studied to increase in the coming decades (Wiel et al. 2024), which can periodically increase groundwater levels (Bresser et al. 2005). However, if a large fraction of the aquifers respond less than proportionately to intense precipitation, this may be an overestimate.

6.3 How strongly are recharge responses related to landscape characteristics?

The large variability in GRRDs (section 5.4) quantifies the spatial heterogeneity of groundwater recharge and its timing. Significant variability is found even in a small area where the mean water table depth has a low range (section 5.5, mean 1.21 m with standard deviation 0.42 m), and the subsurface is dominated by similar types of sand (see table 4 and 6).

Studies on recharge responses in the Netherlands suggest that lag times occur in the magnitude of days to weeks (Zaadnoordijk, Lourens (2019); figure 1, (Wageningen Environmental Research 2025)). Using daily time series and scaled gamma distributions for the IRFs, the median response times in the east of the Netherlands have been found to range from 5 to 100 days, in the central and western Netherlands from 1 to 300 days (Zaadnoordijk et al. 2019). In contrast, The median response times (time of 50% of the total response) of the GRRDs calculated with ERRA are all below 17 hours (mean = 4.2 hours, standard deviation 3.4 hours). The difference between these findings may be due in part to the temporal resolution of the input data. Also, lag times in this study have been deliberately limited to 48 hours to focus on peak responses. However, this also shows that predefined and data-based IRFs can show distinctly different recharge responses, and that the initial recharge response may occur faster than previously assumed. The different median lag times suggest that the tailing behavior of recharge should also be investigated more closely.

Here, the locations are roughly divided into sandy and clay soils. Not knowing the specific yield of the aquifers, the comparison is limited to to water table rise instead of recharge volume (section 2.2). Globally, soil texture alone has little explanatory power on recharge responses, but this can depend on land cover (Kim, Jackson 2012). In regional comparisons, higher recharge rates are found in coarser soils (Cook, Walker (1990), Salem et al. (2023)). Yet in shallow aquifers, capillary rise and increased evaporation can diminish this difference (Koirala et al. (2019), Boumis et al. (2022)).

How the thickness of the unsaturated zone affects groundwater recharge remains under-explored. This study finds that lag times of recharge responses increase with water table depth (section 5.4, figure 13), which is consistent with existing studies (Szilagyi et al. (2013), Guillaumot et al. (2022)). The

relationship between water table depths and the total recharge response appears more ambiguous: though in general recharge is found to decrease with thicker unsaturated zones (Cao et al. (2016), Siyuan et al. (2020), Guillaumot et al. (2022)), it becomes depth-independent at variable depths (2.4 m (Siyuan et al. 2020), 8 m (Szilagyi et al. 2013)). This study has found no consistent relationship between recharge responses and mean water table depths. Comparisons with antecedent water table depth prior to precipitation are not conducted due to time restraints. However, they may offer clearer insights than using the mean water table depth, and are highly recommended for further analysis.

Although this study finds that soil type and mean water table depth wield some influence on recharge responses (section 5.4), the variability within these parameters remains large. Thus, they cannot be used to estimate the size or timing of recharge responses. Larger data sets with a finer distinction between soil properties and with a larger range of water table depths should be tested to investigate the influence of the unsaturated zone in more detail.

6.4 How strongly does recharge response vary between summer and winter?

Some influences on groundwater recharge vary in time, such as evapotranspiration and soil moisture (Xie et al. (2018), Mathias et al. (2017), Boumis et al. (2022)). ERRA has the option to divide the responses by multiple nested conditions. However, such an analysis is restricted by data availability. Therefore, this study compares seasonal GRRDs that summarize multiple forcings and their intercorrelations. Where suitable time series of ambient forcings exist, ERRA could be used to quantify how individual forcings affect the response of the unsaturated zone.

Like several other studies (Jasechko et al. (2014), Jasechko et al. (2017), O'driscoll et al. (2005)), this study observes higher recharge responses during winter months (section 5.6, figure 15). During spring and summer, increased evapotranspiration can reduce the amount of water available for recharge (Sobaga et al. (2024), Boumis et al. (2022)) and the moisture content of the soil. In turn, the reduced soil moisture content further limits the percolation of soil water into the aquifer (Lai et al. (2016), Farmer et al. (2003)).

Soil moisture content could also explain why the summer / winter ratios of the recharge responses differ significantly between soil types. Because the water retention capacity declines for coarser soils (Yang et al. 2023), it can be assumed that the soil moisture content during summer is lower in sandy locations compared to clay locations. In addition, higher capillary rises in clay can lead to increased evaporation and therefore decreased recharge (Koirala et al. 2019). Both factors could explain the significant difference in the recharge seasonality of sandy and clay aquifers (figure 16).

As climate change is expected to shift precipitation towards winter (Hurk et al. (2014), Bresser et al. (2005)), the higher recharge response in wintertime is likely to increase the total amount of winter recharge. During summer, however, soil moisture deficits are likely to increase (Ardilouze et al. (2019), Grillakis (2019)). In addition, more frequent occurrences of extreme precipitation are predicted (Hosseinzadehtalaei et al. (2020), Eden et al. (2018), Wiel et al. (2024)), to which some aquifers appear to respond less than proportionally. Thus, not only the amount of precipitation might decline, but also the summer recharge per unit of precipitation. However, the time series used in this study are not long enough to fully represent the current climate. In addition, the relationship between recharge responses and precipitation intensity should be tested for seasonal NRFs in case the observed non-linearity varies in time.

7 Conclusion

In the 36 shallow aquifers under investigation, the response of groundwater recharge to precipitation varies with space, time, and precipitation intensity. This study quantifies these influences for 36 shallow aquifers in the Netherlands using the recently developed Ensemble Rainfall-Runoff Analysis (ERRA) method. The approach allows to estimate ensemble-averaged Groundwater Recharge Response Distributions (GRRDs).

Calculating the total recharge response for the precipitation ranges of distinct NRFs shows that the recharge increases proportionally (53 %) or less than proportionally (38 %) with precipitation intensity. This implies that intense precipitation events could be a weaker forcing of groundwater recharge than previously assumed in the Netherlands.

Although recharge characteristics are weakly correlated with soil and mean water table depth, their substantial spatial variability limits their use for upscaling. The variability might be lowered by including additional parameters, such as the distance to surface water bodies, but is often restrained by data availability.

In 34 of 36 sites, the average recharge is lower in summer than in winter. This ratio of recharge responses is significantly more pronounced in sandy soils ($p = 0.001$). This implies that climate change can lead not only to reduced amounts of summer precipitation but also to diminished groundwater recharge efficiency, since a smaller fraction of rainfall is likely to become recharge. As seasons combine interdependent physical processes, partitioning the GRRDs by evaporation rates, soil moisture content, and antecedent water table depths could provide a more nuanced analysis of these controls.

Overall, this study underscores the need to further quantify environmental controls on groundwater recharge, with particular attention to their variability in time and space.

Acknowledgments

I want and need to thank my direct supervisor, Wouter Berghuijs. Throughout the whole study, he listened to me with great patience, always offering new perspectives, challenging presumptions, suggesting new experiments. This thesis is built on his contagious curiosity and attention to detail.

I am immensely grateful to James Kirchner, the developer of ERRA, for his kind support and in-depth answers to all my questions.

For information of the Cabauw research site, I exchanged emails with Claudia Brauer, Arnoud Apituley, Mariska Koning and Reinder Ronda, whom I want to thank sincerely for sharing their specific local knowledge with me. Among other things, they provided information on the measurement setups and surface elevations. Figure 4 was supplied by Mariska Koning. Thank you for your support!

The initial search for groundwater time series was supported by Jose David Heano Casas, who shared with me his very useful insights into the workings of DINOloket and hydropandas. And I was lucky in my fellow students, especially Thijs Bollen and Max van Gorkum, who also worked with ERRA. Our discussions on Life, Debugging and Everything made this study more fun and more fruitful.

I have used the chatbot chatgpt.com in accordance with university guidelines (Free University Amsterdam n.d.) to debug my own Python code and suggest improvements to graphs and occasional wording. I declare that this thesis is my own, original work and that I have not used any sources or aids other than those stated.

A Measurement locations

Table 4 describes the groundwater head time series used in this study, as well as their landscape parameters mean water table depth and the predominant soil type. Additionally, it includes distance to the closest surface water body, which is a rough and incomplete estimate from multiple maps and not used for systematic analysis. The table aims to provide an overview; for coordinates, BRO ID numbers and the assigned rain gauges see table 5. Table 6 focuses on the soil core measurements (DINOloket 2022) that are used to characterize subsurface conditions. They describe the subsurface soil at or within 50 m of the well location.

Table 4: Overview of wells where recharge response is analyzed. The wells are roughly divided into geographical regions. Soil type is based on borehole data within 200m of the well (see table 6). Land cover lists the three prevailing land uses in 2023. Distance to closest surface water body should be treated as a rough estimate.

region	name	period [mm/yyyy]	surface [m + NAP]	mean wtd [m]	amplitude [m]	distance surface water [km]	soil type [-]	land cover [-]
Southeast	Aalten	01/2016 - 02/ 2025	19.04	2.15	1.38	0.310	sand/sand	mixed forest, grassland, greenhouses
Southeast	Azewijn	01/2016 - 01/2025	14.81	1.84	1.1	0.042	clay/sand	grassland, greenhouses, confers
Southeast	Beltrum	01/ 2016 - 02/ 2025	18.83	1.72	1.07	0.225	sand/loam	greenhouses, orchards, conifers
Southwest	Gorinchem-1	11/2014-06/2020	0.04	1.29	0.77	0.012	clay/peat	acres, greenhouses, recreation
Southwest	Gorinchem-2	11/2014-06/2020	0.79	0.91	0.27	0.012	clay/peat	acres, greenhouses, recreation
Cabauw	GWL4	08/2003-10/2011	-0.72	0.57	0.44		clay/peat	conifers, acres, greenhouses
Cabauw	GWL5	08/2003-10/2011	-0.83	0.41	0.45		clay/peat	conifers, acres, greenhouses
Cabauw	GWL8	08/2003-10/2011	-0.65	0.45	0.42		clay/peat	conifers, acres, greenhouses
Cabauw	GWLWNN-a	09/2000-11/2024	-0.74	0.48	0.43		clay/peat	conifers, acres, greenhouses
Cabauw	GWLWNS-a	09/2000-11/2024	-0.74	0.013	0.08		clay/peat	conifers, acres, greenhouses
Southeast	Haaksbergen	01/ 2016 - 02/ 2025	29.43	1.27	1.2	0.257	sand/loam	acres, greenhouses, heath
Southwest	Herwijnen-1	10/2007-07/2023	1.38	2.57	0.25	0.021	clay/clay	greenhouses, conifers, heath
Southwest	Herwijnen-2	10/2007-07/2023	2.26	2.49	0.11	0.021	clay/clay	greenhouses, recreation, mixed forest
Southeast	LaagKeppel	05/2015-04/2025	10.46	1.35	0.44	0.100	clay/sand	greenhouses, grassland, mixed forest
Southwest	Langendijk-1	02/2012-07/2023	0.79	1.33	0.4	0.120	clay/clay	fruit farms, conifers, greenhouses
Southeast	Stelkampsveld	02/2017-01/2025	13.92	1.51	0.93	0.253	sand/loam	nature, swamp, heath
Southeast	StelkampsveldBeekvliet	02/2017-03/2025	14.53	1.56	0.82	0.064	sand/sand	heath, grassland, conifers
Southeast	StelkampsveldBorculoseweg34	02/2017-02/2025	14.27	1.11	0.89	0.412	sand/sand	heath, nature, grassland
Southeast	StelkampsveldBorculoseweg44	02/2019-05/2025	14.43	1.12	0.72	0.029	sand/sand	mixed forest, heath, grassland
Southeast	StelkampsveldBosheurneweg	02/2017-03/2025	14.74	1.41	1.03	0.042	sand/sand	nature, heath, conifers
Southeast	StelkampsveldEnteldijk	02/2017-03/2025	13.51	0.85	1.02	0.164	sand/sand	greenhouses, heath, mixed forest
Southeast	StelkampsveldHaytinksdijk	02/2019-05/2025	15.42	1.19	1.17	0.103	sand/sand	heath, grassland, mixed forest
Southeast	StelkampsveldHazelberg7a	02/2019-05/2025	13.38	0.78	0.93	0.010	sand/sand	heath, grassland, mixed forest
Southeast	StelkampsveldHofteweg	02/2019-05/2025	15.17	1.16	1.08	0.236	sand/sand	mixed forest, heath, grassland
Southeast	StelkampsveldLenderiet4	02/2019-05/2025	14.35	1.18	0.95	0.070	sand/sand	heath, grassland, mixed forest
Southeast	StelkampsveldLenderiet7	02/2017-03/2025	15.84	2.42	1.08	0.245	sand/sand	greenhouses, orchards, grassland
Southeast	StelkampsveldMolenweg	02/2019-05/2025	14.26	1.11	1.1	0.013	sand/sand	heath, grassland, mixed forest
Southeast	StelkampsveldWiechersweg	02/2019-05/2025	15.06	0.99	1.11	0.356	sand/sand	mixed forest,heath, grassland
Veenkampen	Veenkampen	06/2011-02/2025	5.70	0.46	0.37		clay/peat	swamp, conifers, recreation
Southeast	Willinks-Bekeringweg	04/2017-04/2025	44.27	1.62	1.23	0.302	sand/sand	greenhouses, orchards, grassland
Southeast	Willinks-Steengroeveweg	04/2017-04/2025	42.93	0.91	1.14	0.414	sand/clay	heath, orchardm grassland
Southwest	Zeek-2	11/2014-06/2020	2.69	2.15	0.46	0.005	clay/peat	fruit farms, recreation, conifers
Southeast	Zelhem-Eeltinkweg	05/2015-04/2025	13.16	1.25	0.69	0.169	sand/sand	beetroot, mixed forest, greenhouse
Southeast	Zelhem-Jolinkdijk	08/2013-01/2024	16.86	1.17	1.2	0.167	sand/sand	heath, greenhouses, swamp
Southwest	Zeving-1	11/2014-03/2020	0.77	1.52	0.44	0.011	clay/sand	buildings, recreation, urban
Southwest	Zeving-3	11/2014-01/2020	1.60	1.65	0.34	0.011	clay/sand	buildings, recreation, urban

Table 5: Well locations and their matched precipitation gauge. The x and y values refer to the Amersfoort RD coordinate system. Distance is the distance between well and gauge.

region	site	(BRO) ID	missing values [%]	x [m]	y [m]	P station name / ID	missing values [%]	distance well-precipitation km
Southeast	Aalten	GMW000000016771	0.00	230576	437115	Neerslagmeter Varsselder (WRIJ)	2.35	≈ 9
Southeast	Azewijn	GMW000000017132	3.72	217059	433200	Neerslagmeter Varsselder (WRIJ)	2.01	4.63
Southeast	Beltrum	GMW000000017237	0.00	233887	450792	Neerslagmeter Harreveld (WRIJ)	11.13	6.29
Southwest	Gorinchem-1	B38H0235-1	0.03	130410	427720	Weerstation Herwijnen (KNMI)	0.00	8.09
Southwest	Gorinchem-2	B38H0235-2	4.21	130410	427720	Weerstation Herwijnen (KNMI)	0.00	8.09
Cabauw	GWL4		3.92	123326	442515	Neerslagmeter Cabauw	0.00	<0.2
Cabauw	GWL5		5.34	123326	442515	Neerslagmeter Cabauw	0.00	<0.2
Cabauw	GWL8		3.25	123326	442515	Neerslagmeter Cabauw	0.00	<0.2
Cabauw	GWLWNN-a		0.00	123326	442515	Neerslagmeter Cabauw	0.00	<0.2
Cabauw	GWLWNS-a		0.00	123326	442515	Neerslagmeter Cabauw	0.00	<0.2
Southeast	Haaksbergen	GMW000000017221	5.47	248528	462263	Neerslagmeter Buurse (WRIJ)	4.15	5.46
Southwest	Herwijnen-1	B38H0384-1	8.00	137170	429230	Weerstation Herwijnen (KNMI)	0.00	1.35
Southwest	Herwijnen-2	B38H0384-2	6.34	137170	429230	Weerstation Herwijnen (KNMI)	0.00	1.35
Southeast	LaagKeppel	GMW000000016984	1.94	210712	444055	Neerslagmeter Wehl (WRIJ)	10.11	2.64
Southwest	Langendijk-1	B38H2377	13.59	136960	431611	Neerslagmeter Wehl (WRIJ)	0.00	2.17
Southeast	Stelkampsveld	GMW000000016832	3.14	230006	459406	Neerslagmeter Borculo (WRIJ)	5.56	2.07
Southeast	StelkampsveldBeekvliet	GMW000000016677	0.00	230180	460230	Neerslagmeter Borculo (WRIJ)	5.56	2.21
Southeast	StelkampsveldBorculoseweg34	GMW000000017122	0.28	229948	459728	Neerslagmeter Borculo (WRIJ)	5.56	2.25
Southeast	StelkampsveldBosheurneweg	GMW000000017231	0.04	22793	458572	Neerslagmeter Borculo (WRIJ)	5.56	4.22
Southeast	StelkampsveldEnteldijk	GMW000000066662	0.75	229405	458446	Neerslagmeter Borculo (WRIJ)	5.56	2.77
Southeast	StelkampsveldLenderiet7	GMW000000016816	0.00	228774	460283	Neerslagmeter Borculo (WRIJ)	5.56	3.54
Southeast	StelkampsveldBorculoseweg44	GMW000000016883	0.00	230517	459655	Neerslagmeter Borculo (WRIJ)	5.61	1.67
Southeast	StelkampsveldLenderiet4	GMW000000017035	1.46	228354	459200	Neerslagmeter Borculo (WRIJ)	5.62	3.70
Southeast	StelkampsveldHaytinksdijk	GMW000000003843	3.17	228735	458050	Neerslagmeter Borculo (WRIJ)	5.60	3.518
Southeast	StelkampsveldHazelberg7a	GMW000000017036	0.74	228902	460623	Neerslagmeter Borculo (WRIJ)	5.61	3.516
Southeast	StelkampsveldWiechersweg	GMW000000017017	0.00	230032	457976	Neerslagmeter Borculo (WRIJ)	5.61	2.34
Southeast	StelkampsveldMolenweg	GMW000000017078	0.10	227845	459305	Neerslagmeter Borculo (WRIJ)	5.62	4.29
Southeast	StelkampsveldHofteweg	GMW000000017003	0.59	228885	457867	Neerslagmeter Borculo (WRIJ)	5.61	3.444
Veenkampen	Veenkampen		0.26	171026	443677	Veenkampen P_1_1_1 (MAQ)	0.86	0.05
Southeast	Willinks-Bekeringweg	GMW000000016722	0.14	251553	442612	Neerslagmeter Ratum-Henxel	1.01	1.49
Southeast	Willinks-Steengroeveweg	GMW000000016785	0.00	251713	442356	Neerslagmeter Ratum-Henxel	1.01	1.25
Southwest	Zeek-2	B38H0254-2	0.70	138950	426750	Weerstation Herwijnen (KNMI)	0.00	3.184
Southeast	Zelhem-Eeltinkweg	GMW000000016695	1.04	218482	445822	Neerslagmeter Hengelo (WRIJ)	0.00	6.41
Southeast	Zelhem-Jolinkdijk	GMW000000079376	7.72	223170	445260	Neerslagmeter Hengelo (WRIJ)	0.00	6.96
Southwest	Zeving-1	B38H0234-1	4.71	134736	428059	Weerstation Herwijnen (KNMI)	0.00	3.994
Southwest	Zeving-3	B38H0234-3	0.03	134736	428059	Weerstation Herwijnen (KNMI)	0.00	3.994

Table 6: Soil information, either directly at the well location or within 200m of it, based on DINOloket data. For Veenkampen and Cabauw wells, soil information is extracted from metadata.

region	site	(BRO) ID	soil information	soil type [-]	borehole ID
Southeast	Aalten	GMW000000016771	different medium sand layers	sand/sand	B41D0127
Southeast	Azewijn	GMW000000017132	2m clay, then fine sand	clay/sand	B40H1475
Southeast	Beltrum	GMW000000017237	very fine sand, loam betw. -0.8 and -1.3m	sand/loam	B34D1413
Southwest	Gorinchem-1	B38H0235-1	clays, 1.2-4.6 peat, clay, coarse sand from -8.6	clay/peat	B38H0235
Southwest	Gorinchem-2	B38H0235-2	clays, 1.2-4.6 peat, clay, coarse sand from -8.7	clay/peat	B38H0235
Cabauw	GWL4	GWL4	∼1.5m clay	clay/peat	metadata
Cabauw	GWL5	GWL5	∼1.5m clay	clay/peat	metadata
Cabauw	GWL8	GWL8	∼1.5m clay	clay/peat	metadata
Cabauw	GWLWNN-a	GWLWNN	∼1.5m clay	clay/peat	metadata
Cabauw	GWLWNS-a	GWLWNS	∼1.5m clay	clay/peat	metadata
Southeast	Haaksbergen	GMW000000017221	fine to medium sand, loam from -2.4	sand/loam	B34G1384
Southwest	Herwijnen-1	B38H0384-1	clay, very coarse sand from -7.1	clay/clay	B38H0136
Southwest	Herwijnen-2	B38H0384-2	clay, very coarse sand from -7.2	clay/clay	B38H0136
Southeast	LaagKeppel	GMW000000016984	very sandy clay, 0.8-1.1 clay, then sand	clay/sand	B40F1951
Southwest	Langendijk-1	B38H2377	very sandy clay, 0.8-1.1 clay, then sand	clay/clay	B38H2628
Southeast	Stelkampsveld	GMW000000016832	medium to fine sand, loam from -3.1	sand/loam	B34C1238
Southeast	StelkampsveldBeekvliet	GMW000000016677	moderately silty sand	sand/sand	BHR000000122860
Southeast	StelkampsveldBorculoseweg34	GMW000000017122	medium fine to very coarse sand	sand/sand	B34C1238
Southeast	StelkampsveldBosheurneweg	GMW000000017231	medium fine to medium coarse sand	sand/sand	B34C0692
Southeast	StelkampsveldEnteldijk	GMW000000066662	moderately silty sand	sand/sand	BHR000000292825
Southeast	StelkampsveldLenderiet7	GMW000000016816	medium to very fine sands	sand/sand	B34C0687
Southeast	StelkampsveldBorculoseweg44	GMW000000016883	medium fine to medium coarse sand; 0.3-0.8 peat?	sand/sand	B34D0991
Southeast	StelkampsveldLenderiet4	GMW000000017035	medium fine to very coarse sand	sand/sand	B34C0731
Southeast	StelkampsveldHaytinksdijk	GMW000000003843	medium to very fine sands	sand/sand	B34C1197
Southeast	StelkampsveldHazelberg7a	GMW000000017036	medium fine to medium coarse sand	sand/sand	B34C0779
Southeast	StelkampsveldWiechersweg	GMW000000017017	medium to very fine sands	sand/sand	B34D0919
Southeast	StelkampsveldMolenweg	GMW000000017078	medium to very fine sands	sand/sand	B34C0726
Southeast	StelkampsveldHofteweg	GMW000000017003	medium to very fine sands	sand/sand	B34C1197
Veenkampen	Veenkampen		0-0.6m clay, below peat	clay/peat	metadata
Southeast	Willinks-Bekeringweg	GMW000000016722	sand, first 30 cm very silty	sand/sand	BHR000000147784
Southeast	Willinks-Steengroeveweg	GMW000000016785	sand, 1.8-1.85 lime stone,grey clay, from 3.32 mergel, from 11.7 limestone	sand/clay	B41F0089
Southwest	Zeek-2	B38H0254-2	diff. Clay types, peat -3.8-5 m, clay again, sand	clay/peat	B38H0254
Southeast	Zelhem-Eeltinkweg	GMW000000016695	medium and coarse sand	sand/sand	B40F1952
Southeast	Zelhem-Jolinkdijk	GMW000000079376	moderately silty sand	sand/sand	BHR000000147327
Southwest	Zeving-1	B38H0234-1	clay, first meter "sandy", coarse sand from -8m	clay/sand	B38H0234
Southwest	Zeving-3	B38H0234-3	clay, first meter "sandy", coarse sand from -8m	clay/sand	B38H0234

B Data access

By region, the following data sets are utilized:
West:

- individual well time series downloaded from Vitens Lizard Viewer (Lizard Viewer 2025)
- precipitation data by the Royal Nederlands Meteorological Institute (Royal Netherland Meteorological Institute (KNMI) 2025c)

Cabauw:

- cesar_groundwater_levelhourly_la1_t1h_v1.0: GWL4, GWL5, GWL8 groundwater time series, gap-filled to 1 hour frequency (Wageningen University 2025)
- KNMI automated weather station 348 (Cabauw): precipitation time series of 1 hour frequency (Royal Netherland Meteorological Institute (KNMI) 2025c)
- cesar_soil_water_lb1_t10_v1.1: GWLWNN and GWLWNS groundwater time series and TH03 soil moisture content (Royal Netherland Meteorological Institute (KNMI) 2025a)
- cesar_surfac_meteo_lc1$\widehat{10}$_v1.0: precipitation time series of 10 minutes frequency (Royal Netherland Meteorological Institute (KNMI) 2025b)

Veenkampen: METEOROLOGY and SOIL datasets downloaded from Ruisdael Observatory website (MAQ Observations - Data Downloads) 2025) East:

- Waterschap Rijn en IJssel: individual well and precipitation time series (Waterschap Rijn end IJssel 2025)
- soil moisture network Twente: ITCSM stations (Velde 2022)
- maps of water ways ('Leidingvak' and 'Watergang') for estimating the distance to the closest surface water body (Waterschap Rijn end IJssel 2024)

The pre-processed time series files and the output files created by ERRA can be found here: `https://drive.google.com/drive/folders/1tAS0oHjt_oDoF-XQvAqXMGSuXy7L7WVs?usp=sharing`

C Groundwater Recharge Response Distributions (GRRDs)

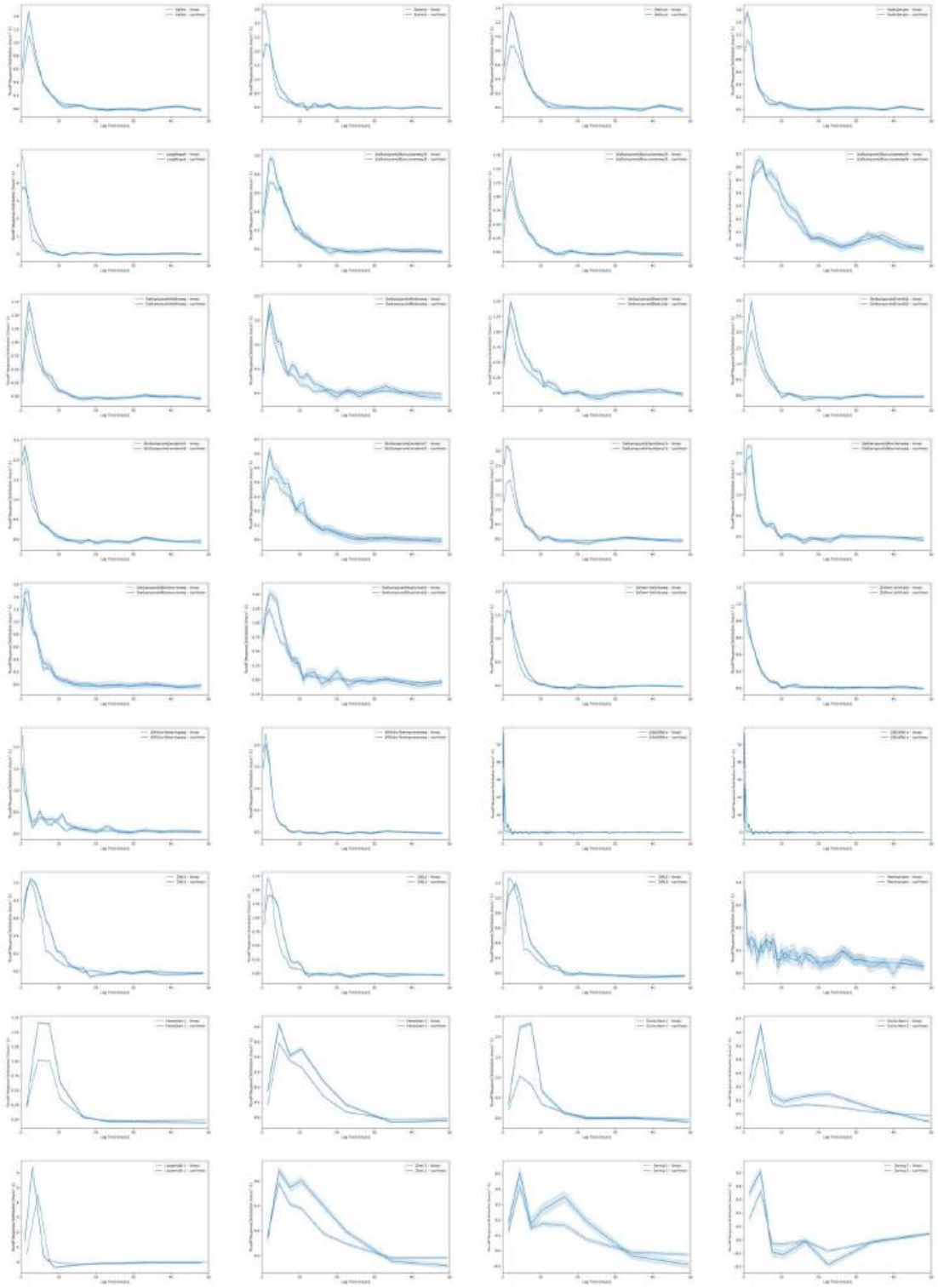

Figure 17: Ensemble-averaged GRRDs of all wells, linear (dashed line) and nonlinear (solid line). Note that the y-axes of the subplots differ. The shaded areas represent ± 1 standard error.

Table 7: Shape parameters of ensemble-averaged, precipitation-weighted GRRDs: peak response time (tpeak [hour]), peak response (peakht [hour^{-1}]), peak width (width [hour]), and total response (rc [-]), with standard errors _se

site	tpeak	tpeak_se	peakht	peakht_se	width	width_se	rc	rc_se
Aalten	2.04	0.02	1.47	0.03	3.68	0.18	6.70	0.25
Azewijn	1.50	0.07	2.31	0.08	3.59	0.15	10.06	0.56
Beltrum	2.52	0.12	1.33	0.07	4.51	0.23	6.84	0.27
Gorinchem-1	6.17	0.04	2.50	0.05	6.80	0.11	18.14	0.88
Gorinchem-2	4.33	0.06	0.66	0.02	4.35	0.22	6.09	0.32
GWL4	3.26	0.11	1.05	0.03	6.59	0.29	7.43	0.20
GWL5	2.79	0.11	1.44	0.05	5.38	0.16	7.95	0.30
GWL8	3.15	0.08	1.19	0.03	5.71	0.23	7.90	0.21
GWLWNN-a	0.36	0.02	28.11	3.39	0.48	0.04	20.56	0.86
GWLWNS-a	0.36	0.02	28.11	3.39	0.48	0.04	20.55	0.86
Haaksbergen	1.51	0.19	1.67	0.40	2.48	0.28	5.46	0.31
Herwijnen-1	6.28	0.12	1.81	0.08	7.12	0.17	13.48	0.32
Herwijnen-2	5.04	0.06	0.63	0.02	12.05	0.37	7.69	0.19
LaagKeppel	1.56	0.24	4.07	1.11	3.00	0.62	13.72	0.56
Langendijk-1	3.39	0.01	6.53	0.08	2.89	0.04	19.34	0.63
Stelkampsveld	2.65	0.09	1.01	0.05	5.57	0.36	6.14	0.35
StelkampsveldBeekvliet	2.49	0.15	1.44	0.12	4.62	0.49	8.96	0.43
StelkampsveldBorculoseweg34	1.95	0.02	1.72	0.04	3.40	0.19	7.18	0.35
StelkampsveldBorculoseweg44	4.63	0.38	0.64	0.04	10.21	0.80	7.62	0.39
StelkampsveldBosheurneweg	1.65	0.08	1.57	0.09	3.86	0.32	6.84	0.59
StelkampsveldEnteldijk	2.06	0.02	2.98	0.05	3.52	0.18	11.93	0.56
StelkampsveldHaytinksdijk	2.77	0.19	1.52	0.07	5.60	0.34	9.97	0.81
StelkampsveldHazelberg7a	1.67	0.18	3.56	0.66	3.23	0.36	12.21	0.67
StelkampsveldHofteweg	2.42	0.17	1.66	0.17	3.84	0.31	7.96	0.40
StelkampsveldLenderiet4	1.59	0.22	2.50	0.62	3.09	0.62	8.65	0.50
StelkampsveldLenderiet7	2.09	0.09	0.63	0.04	7.22	0.35	5.27	0.37
StelkampsveldMolenweg	2.14	0.06	1.85	0.09	4.23	0.39	11.62	0.85
StelkampsveldWiechersweg	1.53	0.04	2.29	0.06	3.07	0.18	7.97	0.61
Veenkampen	0.55	0.02	0.42	0.05	0.68	0.12	3.48	0.29
Willinks-Bekeringweg	0.59	0.01	1.88	0.09	1.41	0.17	8.23	0.56
Willinks-Steengroeveweg	1.19	0.02	2.06	0.04	2.36	0.03	5.37	0.24
Zeek-2	9.78	1.24	0.66	0.12	15.49	1.87	10.84	0.48
Zelhem-Eeltinkweg	1.74	0.23	1.82	0.36	4.04	0.64	7.04	0.32
Zelhem-Jolinkdijk	0.60	0.01	1.43	0.03	1.94	0.13	3.46	0.20
Zeving-1	4.49	0.14	0.51	0.04	4.62	0.53	7.41	0.57
Zeving-3	3.63	0.15	0.54	0.04	4.68	0.22	2.67	0.45

D Nonlinear Response Functions (NRFs)

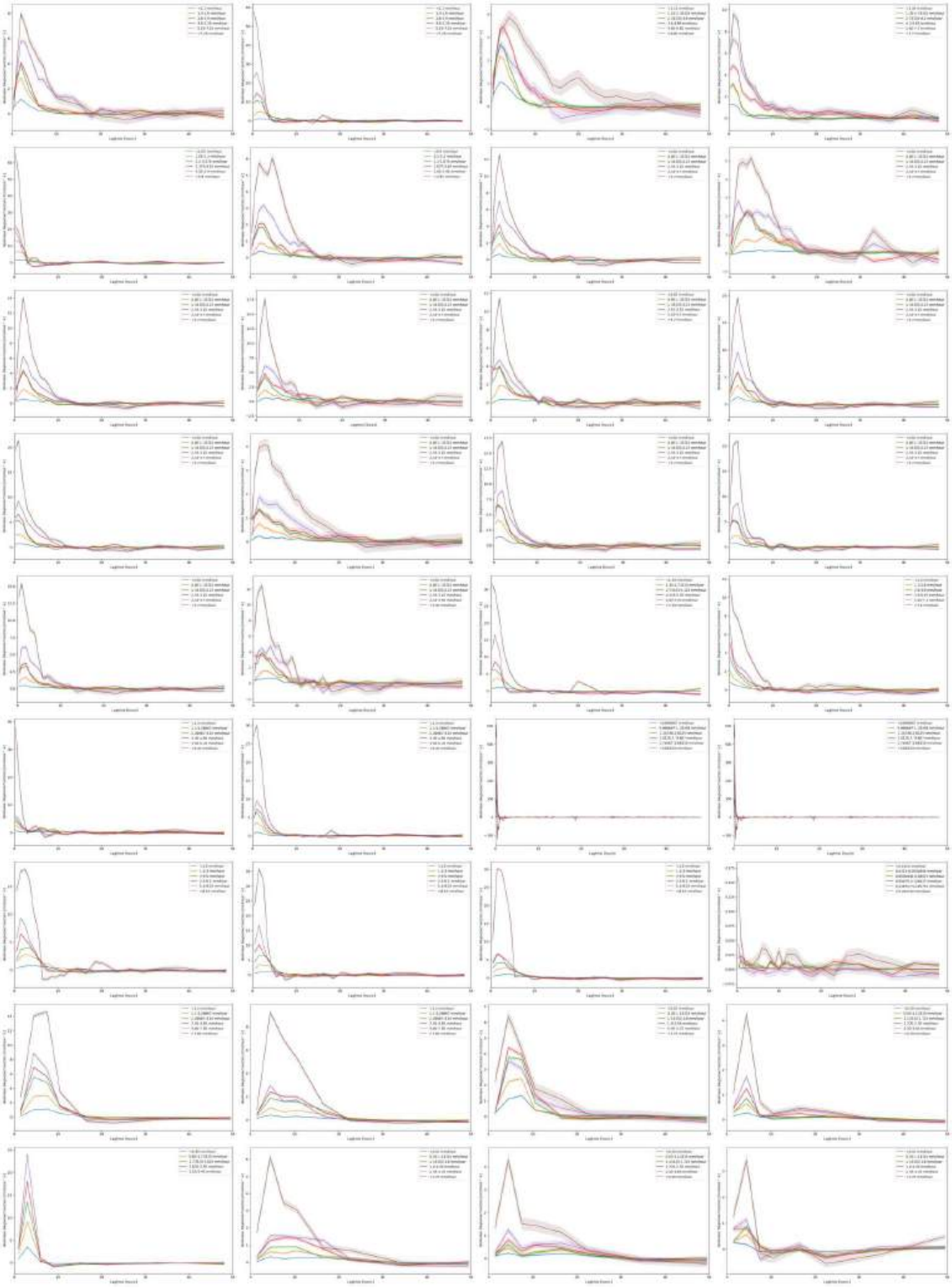

Figure 18: Nonlinear Response Functions for 6 evenly spaced precipitation segments (5 xknots). The shaded areas represent ± 1 standard error. Note that the y-axes of the subplots differ.

E Linearity analysis

Figure 19: Power law (red) and linear (black) fit to total recharge response ('rsum') over precipitation intensity. The shaded areas represent ± 1 standard error.

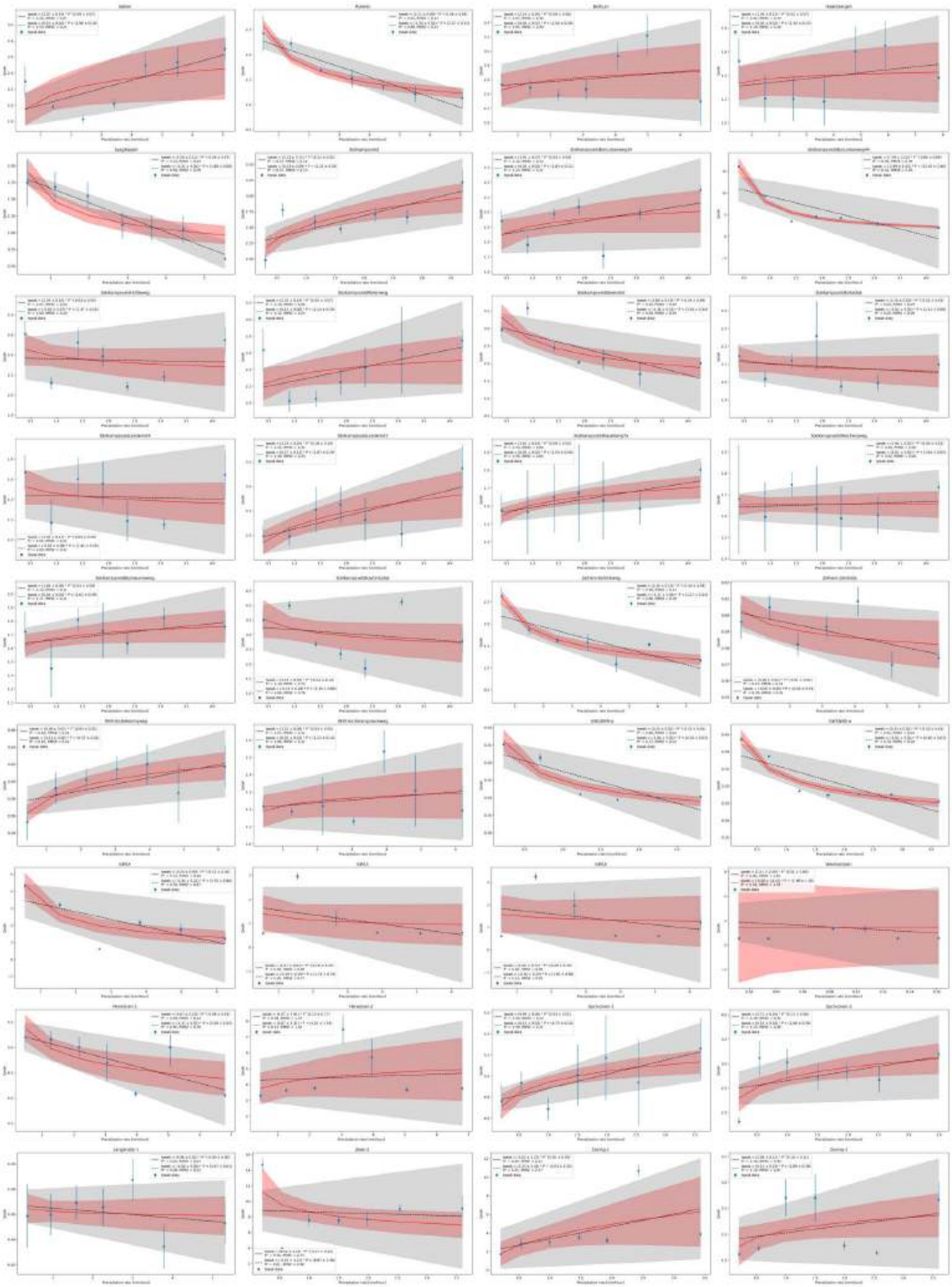

Figure 20: Power law (red) and linear (black) fit to peak response time ('tpeak') over precipitation intensity. The shaded areas represent ± 1 standard error.

Table 8: Linearity analysis of the total recharge response. The parameters of the power law and linear fit a and n, as well as their standard errors n_{se} and a_{se}, coefficient of determination R^2, and Root Mean Square Error $RMSE$.

	$response = (a \pm a_{se}) * P^{n \pm n_{se}}$						$response = (a \pm a_{se}) * P$			
site	a	a_{se}	n	n_{se}	R^2	$RMSE$	a	a_{se}	R^2	$RMSE$
Aalten	2.70	1.19	1.51	0.25	0.94	3.98	6.41	0.53	0.89	5.36
Azewijn	6.35	2.19	1.38	0.20	0.95	6.29	11.99	0.82	0.92	8.34
Beltrum	8.91	2.09	0.45	0.16	0.72	3.02	3.79	0.54	0.21	5.04
Haaksbergen	5.15	3.08	1.11	0.33	0.83	7.17	6.25	0.66	0.83	7.26
Stelkampsveld	5.22	0.88	1.22	0.15	0.96	1.54	6.56	0.36	0.95	1.85
LaagKeppel	16.71	3.11	0.63	0.13	0.89	4.63	9.99	0.83	0.77	6.78
Zelhem-Eeltinkweg	3.64	2.61	1.30	0.40	0.79	7.30	6.09	0.72	0.77	7.61
Zelhem-Jolinkdijk	3.50	1.36	0.90	0.24	0.83	2.43	2.97	0.26	0.83	2.47
Willinks-Steengroeveweg	7.86	1.41	0.84	0.12	0.96	2.34	6.14	0.31	0.94	2.76
Willinks-Bekeringweg	12.49	4.94	0.25	0.29	0.19	7.21	4.00	1.11	-0.55	9.93
StelkampsveldBosheurneweg	8.50	2.92	0.98	0.29	0.79	5.15	8.32	0.89	0.79	5.15
StelkampsveldLenderiet4	11.08	3.11	0.98	0.24	0.85	5.48	10.85	0.94	0.85	5.49
StelkampsveldLenderiet7	7.32	2.58	0.78	0.31	0.67	4.32	5.76	0.77	0.64	4.50
StelkampsveldEnteldijk	13.88	3.88	0.85	0.24	0.79	6.60	11.83	1.17	0.78	6.80
StelkampsveldBorculoseweg34	6.53	2.06	1.31	0.25	0.90	4.21	9.26	0.82	0.87	4.80
StelkampsveldBorculoseweg44	10.66	1.58	0.85	0.13	0.93	2.68	9.03	0.52	0.92	3.00
StelkampsveldHaytinksdijk	13.80	3.67	0.66	0.24	0.69	6.05	9.51	1.19	0.59	6.95
StelkampsveldHofteweg	11.00	3.56	0.80	0.29	0.72	5.98	8.79	1.07	0.69	6.25
StelkampsveldBeekvliet	14.81	3.21	0.52	0.21	0.66	5.29	8.79	1.25	0.35	7.29
StelkampsveldMolenweg	18.53	5.20	0.65	0.26	0.68	8.57	12.68	1.71	0.57	9.94
StelkampsveldHazelberg7a	15.60	3.71	0.69	0.21	0.76	6.14	11.18	1.21	0.68	7.05
StelkampsveldWiechersweg	11.15	3.37	0.82	0.26	0.75	5.69	9.14	1.02	0.73	5.92
GWL4	9.68	1.41	0.61	0.10	0.95	1.87	5.30	0.44	0.79	3.76
GWL5	10.56	1.50	0.71	0.09	0.97	2.08	6.73	0.43	0.90	3.70
GWL8	10.36	2.01	0.58	0.13	0.90	2.65	5.39	0.52	0.71	4.55
GWLWNN-a	23.23	6.24	1.49	0.30	0.94	9.11	34.52	3.26	0.89	12.65
GWLWNS-a	32.15	9.08	1.01	0.27	0.87	14.68	32.46	2.84	0.87	14.68
Gorinchem-1	19.92	2.09	0.53	0.11	0.87	3.71	12.91	1.41	0.58	6.78
Gorinchem-2	5.92	0.96	0.70	0.17	0.84	1.62	4.48	0.41	0.77	1.93
Herwijnen-1	18.21	2.68	0.60	0.10	0.93	4.14	9.68	0.86	0.74	8.11
Herwijnen-2	11.99	2.83	0.46	0.16	0.74	4.19	5.13	0.75	0.27	7.06
Langendijk-1	25.33	1.02	0.78	0.03	1.00	1.70	18.86	0.77	0.96	5.50
Zeek-2	12.48	2.40	0.63	0.20	0.78	4.12	8.83	1.07	0.65	5.16
Zeving-1	7.06	1.34	0.84	0.20	0.85	2.23	6.09	0.51	0.83	2.34
Zeving-3	3.08	0.17	0.86	0.06	0.99	0.29	2.69	0.09	0.98	0.42
Veenkampen	0.40	0.57	0.31	0.56	0.10	0.14	1.72	0.68	-0.12	0.16

Table 9: Linearity analysis of the peak response time. The parameters of the power law and linear fit n and a as well as their standard errors n_{se} and a_{se}, coefficient of determination R^2, and Root Mean Square Error $RMSE$

	$response = (a \pm a_{se}) * P^{n \pm n_{se}}$						$response = (a \pm a_{se}) * P + (b \pm b_{se})$					
site	a	a_{se}	n	n_{se}	R^2	$RMSE$	a	a_{se}	b	b_{se}	R^2	$RMSE$
Aalten	2.07	0.19	0.09	0.07	0.25	0.27	0.10	0.04	1.90	0.18	0.53	0.21
Azewijn	2.11	0.09	-0.28	0.04	0.91	0.14	-0.20	0.03	2.37	0.13	0.89	0.15
Beltrum	2.53	0.20	0.04	0.06	0.07	0.30	0.04	0.07	2.50	0.26	0.05	0.30
Haaksbergen	1.36	0.13	0.02	0.07	0.02	0.19	0.03	0.03	1.30	0.15	0.10	0.18
Stelkampsveld	2.53	0.11	0.12	0.05	0.57	0.22	0.23	0.09	2.22	0.19	0.57	0.23
LaagKeppel	1.50	0.11	-0.26	0.07	0.72	0.20	-0.22	0.02	1.88	0.08	0.94	0.09
Zelhem-Eeltinkweg	2.16	0.10	-0.30	0.04	0.90	0.15	-0.17	0.06	2.27	0.24	0.66	0.28
Zelhem-Jolinkdijk	0.60	0.01	-0.01	0.01	0.23	0.01	0.00	0.00	0.60	0.01	0.35	0.01
Willinks-Steengroeveweg	1.22	0.08	0.03	0.05	0.07	0.12	0.02	0.03	1.21	0.10	0.06	0.12
Willinks-Bekeringweg	0.58	0.01	0.04	0.01	0.65	0.01	0.01	0.00	0.57	0.01	0.41	0.02
StelkampsveldBosheurneweg	1.68	0.06	0.03	0.04	0.13	0.11	0.04	0.04	1.62	0.09	0.17	0.11
StelkampsveldLenderiet4	1.46	0.11	-0.05	0.09	0.05	0.22	-0.01	0.08	1.45	0.19	0.00	0.22
StelkampsveldLenderiet7	2.19	0.20	0.18	0.10	0.42	0.35	0.27	0.12	1.87	0.29	0.49	0.33
StelkampsveldEnteldijk	2.10	0.05	-0.01	0.03	0.05	0.09	-0.02	0.03	2.12	0.08	0.05	0.09
StelkampsveldBorculoseweg34	1.91	0.07	0.03	0.04	0.12	0.13	0.05	0.05	1.83	0.11	0.23	0.12
StelkampsveldBorculoseweg44	7.39	0.52	-0.86	0.09	0.96	0.94	-2.99	1.05	12.19	2.48	0.62	2.85
StelkampsveldHaytinksdijk	3.19	0.39	-0.11	0.14	0.10	0.75	-0.13	0.28	3.30	0.68	0.04	0.78
StelkampsveldHofteweg	2.39	0.10	-0.03	0.05	0.07	0.20	-0.01	0.07	2.37	0.18	0.00	0.20
StelkampsveldBeekvliet	2.66	0.19	-0.24	0.09	0.59	0.39	-0.38	0.14	3.18	0.34	0.58	0.39
StelkampsveldMolenweg	2.33	0.14	0.05	0.07	0.10	0.26	0.13	0.08	2.14	0.20	0.32	0.23
StelkampsveldHazelberg7a	1.61	0.03	0.04	0.02	0.43	0.06	0.05	0.02	1.55	0.04	0.54	0.05
StelkampsveldWiechersweg	1.65	0.03	0.00	0.02	0.00	0.06	0.01	0.02	1.64	0.05	0.02	0.06
GWL4	3.24	0.44	-0.51	0.16	0.72	0.66	-0.45	0.22	3.70	0.86	0.50	0.87
GWL5	1.27	0.61	-0.16	0.43	0.05	0.84	-0.19	0.19	1.74	0.76	0.20	0.77
GWL8	1.50	0.72	-0.09	0.40	0.02	0.96	-0.16	0.23	1.92	0.89	0.11	0.91
GWLWNN-a	0.25	0.01	-0.25	0.05	0.86	0.02	-0.06	0.02	0.34	0.03	0.72	0.03
GWLWNS-a	0.33	0.01	-0.20	0.03	0.91	0.02	-0.05	0.01	0.40	0.03	0.70	0.04
Gorinchem-1	4.94	0.06	0.03	0.01	0.50	0.13	0.13	0.05	4.75	0.10	0.59	0.12
Gorinchem-2	2.71	0.16	0.11	0.06	0.39	0.34	0.19	0.16	2.46	0.30	0.23	0.38
Herwijnen-1	5.07	0.20	-0.08	0.03	0.49	0.32	-0.17	0.07	5.28	0.25	0.56	0.30
Herwijnen-2	4.07	0.91	0.10	0.17	0.08	1.37	0.07	0.31	4.25	1.19	0.01	1.42
Langendijk-1	4.46	0.01	0.00	0.00	0.01	0.01	0.00	0.00	4.47	0.01	0.08	0.01
Zeek-2	8.62	1.24	-0.17	0.15	0.16	2.74	-0.22	1.21	8.87	2.38	0.01	2.98
Zeving-1	3.62	1.25	0.45	0.39	0.29	2.32	1.33	1.02	2.03	1.92	0.25	2.37
Zeving-3	2.08	0.21	0.10	0.11	0.16	0.46	0.14	0.19	1.89	0.38	0.10	0.47
Veenkampen	1.51	2.59	0.01	0.60	0.00	1.62	-6.08	14.43	1.96	1.40	0.03	1.59

Table 10: Linearity analysis of the peak response time. The parameters of the power law and linear fit a and n, as well as their standard errors a_{se} and n_{se}, coefficient of determination R^2, and Root Mean Square Error $RMSE$.

	$response = (a \pm a_{se}) * P^{(n \pm n_{se})}$						$response = (a \pm a_{se}) * P$					
site	a	a_{se}	n	n_{se}	R^2	$RMSE$	a	a_{se}	b	b_{se}	R^2	$RMSE$
Aalten	3.49	0.54	0.13	0.11	0.21	0.76	0.28	0.13	3.03	0.54	0.48	0.62
Azewijn	5.03	0.08	-0.46	0.02	0.99	0.14	-0.62	0.18	5.68	0.73	0.71	0.85
Beltrum	3.70	0.80	0.36	0.15	0.53	1.14	0.74	0.19	3.01	0.72	0.75	0.84
Haaksbergen	2.41	0.39	0.19	0.11	0.38	0.54	0.19	0.10	2.24	0.43	0.44	0.51
Stelkampsveld	5.17	0.25	-0.05	0.06	0.15	0.53	-0.03	0.23	5.16	0.48	0.00	0.58
LaagKeppel	3.48	0.11	-0.48	0.03	0.97	0.21	-0.70	0.14	4.65	0.48	0.83	0.55
Zelhem-Eeltinkweg	4.81	0.23	-0.42	0.05	0.94	0.36	-0.54	0.14	5.33	0.63	0.74	0.73
Zelhem-Jolinkdijk	1.87	0.15	-0.06	0.07	0.12	0.23	-0.05	0.05	1.94	0.20	0.17	0.23
Willinks-Steengroeveweg	2.27	0.11	0.08	0.04	0.45	0.17	0.07	0.05	2.21	0.17	0.31	0.19
Willinks-Bekeringweg	1.35	0.15	0.03	0.09	0.03	0.23	-0.01	0.05	1.42	0.20	0.01	0.23
StelkampsveldBosheurneweg	3.68	0.23	-0.03	0.07	0.04	0.44	-0.01	0.16	3.65	0.39	0.00	0.45
StelkampsveldLenderiet4	3.14	0.20	-0.10	0.08	0.24	0.39	-0.09	0.16	3.17	0.38	0.06	0.44
StelkampsveldLenderiet7	7.10	0.61	0.09	0.09	0.14	1.12	0.52	0.38	6.37	0.89	0.28	1.03
StelkampsveldEnteldijk	3.56	0.21	-0.08	0.07	0.20	0.40	-0.12	0.15	3.67	0.36	0.10	0.42
StelkampsveldBorculoseweg34	3.51	0.35	0.10	0.11	0.12	0.63	0.31	0.21	3.07	0.49	0.31	0.56
StelkampsveldBorculoseweg44	6.31	1.68	0.36	0.26	0.31	2.83	1.53	1.04	4.64	2.47	0.30	2.84
StelkampsveldHaytinksdijk	5.29	0.51	0.03	0.11	0.02	0.95	0.25	0.33	4.86	0.79	0.10	0.91
StelkampsveldHofteweg	3.97	0.16	-0.11	0.05	0.51	0.30	-0.16	0.14	4.10	0.34	0.20	0.39
StelkampsveldBeekvliet	5.59	1.10	-0.24	0.24	0.17	2.21	-0.88	0.80	6.83	1.90	0.19	2.18
StelkampsveldMolenweg	4.57	0.55	0.06	0.13	0.03	1.01	0.20	0.37	4.28	0.87	0.06	1.00
StelkampsveldHazelberg7a	3.18	0.10	0.00	0.03	0.00	0.18	0.03	0.06	3.14	0.15	0.03	0.18
StelkampsveldWiechersweg	3.17	0.10	-0.14	0.04	0.71	0.20	-0.25	0.08	3.48	0.20	0.63	0.23
GWL4	7.85	0.25	-0.42	0.03	0.97	0.36	-1.06	0.22	9.14	0.82	0.86	0.84
GWL5	4.94	0.60	-0.37	0.12	0.70	0.87	-0.78	0.08	6.25	0.29	0.96	0.30
GWL8	5.65	0.62	-0.23	0.10	0.57	0.86	-0.56	0.18	6.46	0.71	0.70	0.72
GWLWNN-a	0.41	0.01	-0.43	0.02	0.99	0.02	-0.17	0.05	0.67	0.09	0.70	0.09
GWLWNS-a	0.43	0.01	-0.41	0.02	0.99	0.02	-0.13	0.04	0.64	0.08	0.67	0.10
Gorinchem-1	6.56	0.33	0.02	0.06	0.03	0.73	0.33	0.27	6.06	0.52	0.23	0.65
Gorinchem-2	4.11	0.16	-0.06	0.04	0.29	0.35	-0.30	0.10	4.56	0.20	0.63	0.25
Herwijnen-1	7.56	0.16	-0.18	0.02	0.94	0.27	-0.45	0.13	7.98	0.50	0.71	0.59
Herwijnen-2	12.45	1.04	-0.11	0.07	0.33	1.67	-0.86	0.23	14.11	0.88	0.74	1.05
Langendijk-1	3.30	0.04	-0.02	0.01	0.42	0.07	-0.03	0.02	3.34	0.06	0.33	0.07
Zeek-2	15.40	1.03	-0.17	0.07	0.50	2.28	-1.06	1.23	16.91	2.40	0.13	3.01
Zeving-1	3.97	2.20	1.24	0.54	0.63	3.82	4.79	1.67	0.43	3.15	0.62	3.89
Zeving-3	3.01	0.34	0.12	0.13	0.18	0.73	0.18	0.32	2.79	0.62	0.06	0.78
Veenkampen	2.51	2.98	0.12	0.44	0.02	1.36	-1.67	12.41	1.95	1.20	0.00	1.37

F Seasonal Groundwater Recharge Response Distributions (GRRDs)

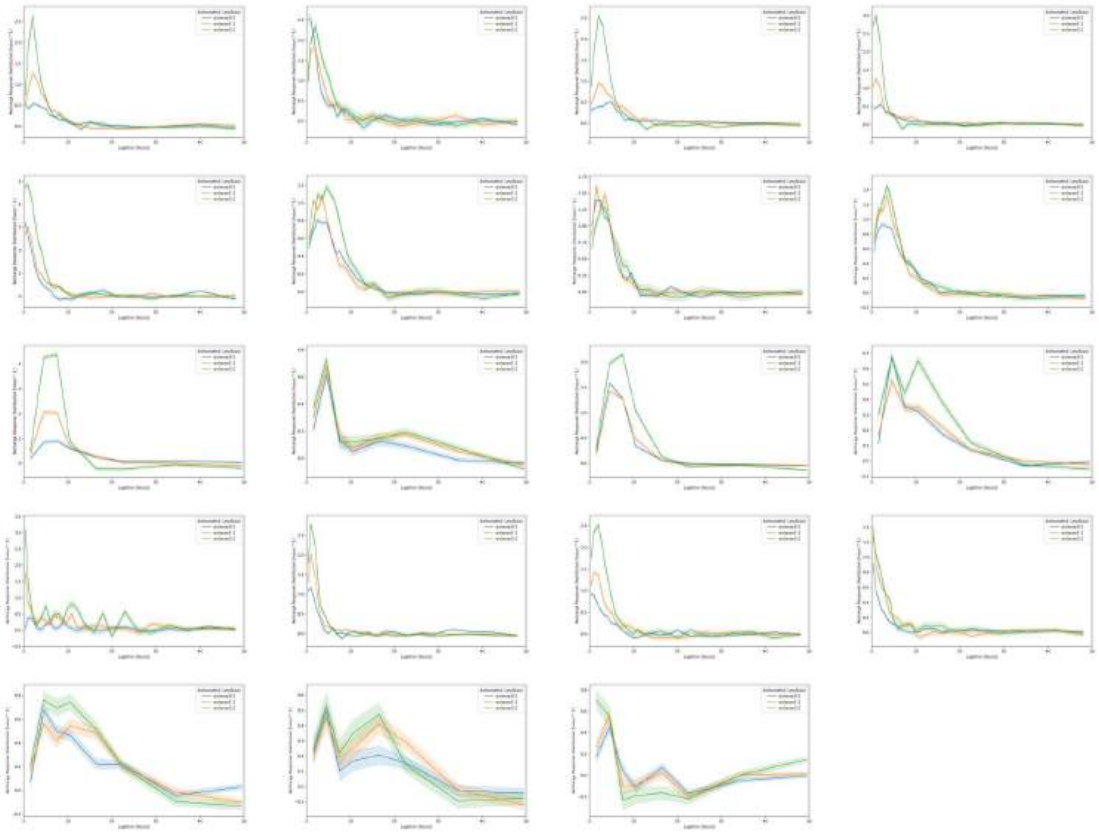

Figure 21: Seasonal GRRDs. Winter (green), summer (blue), and transition periods (orange). The shaded areas represent ± 1 standard error.
Seasonal GRRDs have not been calculated for all aquifers due to diverse limitations: The time series of all Stelkampsveld locations were too short for further division. Similarly, the Langendijk time series contained too many NaN values. For Veenkampen, GWLWNN and GWLWNS sufficient data points were available, but higher computational power would have been required.

Table 11: Summer to winter ratio of total recharge response, peak response, peak response time, and peak width of the GRRDs for summer (s), winter (w), and the summer to winter ratio (r). The sub-scripted *se* is the standard error.

	total response						peak response time						peak rsponse						peak width					
site	s	s_{se}	w	w_{se}	r	r_{se}	s	s_{se}	w	w_{se}	r	r_{se}	s	s_{se}	w	w_{se}	r	r_{se}	s	s_{se}	w	w_{se}	r	r_{se}
Aalten	4.25	0.42	9.63	0.60	0.44	0.05	0.61	0.02	1.96	0.02	0.31	0.01	0.68	0.06	2.65	0.06	0.26	0.02	6.28	0.48	2.84	0.08	2.21	0.18
Azewijn	9.16	0.89	11.37	1.32	0.81	0.12	1.16	0.20	1.94	0.11	0.60	0.11	3.01	0.93	2.40	0.16	1.26	0.40	2.40	0.52	4.10	0.32	0.58	0.14
Beltrum	3.87	0.44	10.51	0.59	0.37	0.05	3.88	0.39	2.45	0.10	1.58	0.17	0.48	0.05	2.53	0.15	0.19	0.02	6.43	0.32	3.79	0.14	1.70	0.11
Gorinchem-1	12.04	1.31	30.80	1.74	0.39	0.05	6.81	0.32	6.10	0.04	1.12	0.05	0.95	0.08	4.76	0.09	0.20	0.02	10.31	1.26	6.52	0.11	1.58	0.19
Gorinchem-2	4.53	0.51	7.50	0.60	0.60	0.08	4.37	0.11	4.10	0.13	1.07	0.04	0.62	0.05	0.74	0.05	0.84	0.09	4.20	0.40	4.29	0.50	0.98	0.15
GWL4	6.23	0.29	9.45	0.52	0.66	0.05	3.36	0.14	4.50	0.20	0.75	0.05	0.81	0.02	1.16	0.05	0.70	0.04	7.50	0.39	7.43	0.41	1.01	0.08
GWL5	7.86	0.41	7.98	0.83	0.99	0.11	2.41	0.29	3.08	0.14	0.78	0.10	1.36	0.10	1.27	0.06	1.07	0.09	5.18	0.18	5.61	0.47	0.92	0.08
GWL8	7.29	0.30	9.33	0.57	0.78	0.06	3.14	0.13	3.40	0.14	0.93	0.05	0.95	0.03	1.39	0.06	0.69	0.04	7.18	0.34	5.47	0.31	1.31	0.10
Haaksbergen	3.61	0.49	8.06	0.68	0.45	0.07	1.77	0.28	1.18	0.18	1.49	0.33	0.60	0.13	3.53	0.92	0.17	0.06	4.41	1.33	2.30	0.35	1.92	0.65
Herwijnen-1	11.02	0.50	18.45	0.72	0.60	0.04	6.00	0.27	6.50	0.07	0.92	0.04	1.58	0.18	2.25	0.05	0.70	0.08	6.32	0.37	8.75	0.97	0.72	0.09
Herwijnen-2	6.43	0.31	10.15	0.46	0.63	0.04	4.90	0.07	4.86	0.16	1.01	0.04	0.69	0.03	0.67	0.04	1.03	0.07	8.05	1.60	15.39	0.74	0.52	0.11
LaagKeppel	10.56	0.94	18.76	1.22	0.56	0.06	1.11	0.24	1.59	0.26	0.70	0.19	3.33	1.37	5.23	1.45	0.64	0.32	2.03	0.81	3.25	0.73	0.63	0.29
Langendijk-1	20.04	0.99	18.62	1.42	1.08	0.10	3.42	0.02	3.26	0.03	1.05	0.01	6.11	0.13	6.32	0.18	0.97	0.03	3.12	0.08	2.96	0.11	1.06	0.05
Willinks-Bekeringweg	3.32	0.92	12.73	1.20	0.26	0.08	1.64	0.19	0.57	0.01	2.88	0.34	0.41	0.13	3.70	0.20	0.11	0.03	1.94	0.44	1.02	0.15	1.89	0.52
Willinks-Steengroeveweg	4.12	0.39	6.99	0.49	0.59	0.07	1.15	0.17	1.26	0.02	0.91	0.13	1.37	0.38	2.88	0.08	0.48	0.13	2.28	0.55	2.30	0.04	0.99	0.24
Zeek-2	9.32	0.73	13.06	0.96	0.71	0.08	5.32	0.20	9.94	1.06	0.54	0.06	0.71	0.05	0.80	0.11	0.88	0.14	10.80	1.09	16.59	1.41	0.65	0.09
Zelhem-Eeltinkweg	3.85	0.46	11.27	0.77	0.34	0.05	1.16	0.21	1.75	0.06	0.67	0.12	1.08	0.35	2.56	0.08	0.42	0.14	3.19	1.38	3.96	0.13	0.81	0.35
Zelhem-Jolinkdijk	2.62	0.28	4.88	0.48	0.54	0.08	0.58	0.01	1.16	0.29	0.50	0.13	1.11	0.04	1.31	0.56	0.84	0.36	1.28	0.14	2.63	1.54	0.49	0.29
Zeving-1	5.69	0.93	8.53	1.18	0.67	0.14	4.23	0.24	4.44	0.33	0.95	0.09	0.50	0.07	0.53	0.09	0.93	0.21	4.30	0.71	18.20	1.35	0.24	0.04
Zeving-3	2.31	0.69	4.43	1.04	0.52	0.20	4.23	0.19	2.79	0.13	1.52	0.10	0.46	0.06	0.89	0.09	0.51	0.08	4.05	0.71	4.52	0.35	0.89	0.17

References

Alsumaiei, Abdullah A. (2020). "A nonlinear autoregressive modeling approach for forecasting groundwater level fluctuation in urban aquifers". In: *Water* 12.3, p. 820. DOI: https://doi.org/10.3390/w12030820.

Ardilouze, Constantin, Batté, Lauriane, Déqué, Michel, Meijgaard, Erik van, Hurk, Bart van den (2019). "Investigating the impact of soil moisture on European summer climate in ensemble numerical experiments". In: *Climate Dynamics* 52, pp. 4011–4026. DOI: https://doi.org/10.1007/s00382-018-4358-1.

Asmuth, Jos R. von, Bierkens, Marc FP., Maas, Kees (2002). "Transfer function-noise modeling in continuous time using predefined impulse response functions". In: *Water Resources Research* 38.12, pp. 23–1. DOI: https://doi.org/10.1029/2001WR001136.

Bakker, Mark, Maas, Kees, Schaars, Frans, Von Asmuth, Jos R. (2007). "Analytic modeling of groundwater dynamics with an approximate impulse response function for areal recharge". In: *Advances in Water Resources* 30.3, pp. 493–504. DOI: https://doi.org/10.1016/j.advwatres.2006.04.008.

Barron, OV., Crosbie, RS., Dawes, WR., Charles, SP., Pickett, T., Donn, MJ. (2012). "Climatic controls on diffuse groundwater recharge across Australia". In: *Hydrology and Earth System Sciences* 16.12, pp. 4557–4570. DOI: https://doi.org/10.5194/hess-16-4557-2012.

Bartholomeus, Ruud P., Wiel, Karin van der, Loon, Anne F. van, Huijgevoort, Marjolein HJ. van, Vliet, Michelle TH. van, Mens, Marjolein, Muurling-van Geffen, Sharon, W.anders, Niko, Pot, Wieke (2023). "Managing water across the flood–drought spectrum: Experiences from and challenges for the Netherlands". In: *Cambridge Prisms: Water* 1, e2. DOI: https://doi.org/10.1017/wat.2023.4.

Becke, AL., Solórzano-Rivas, SC., Werner, AD. (2024). "The watertable fluctuation method of recharge estimation: A review". In: *Advances in Water Resources* 189, p. 104635. URL: https://doi.org/10.1016/j.advwatres.2024.104635.

Bense, Victor, Teuling, Adriaan, Mustafa, Syed, Ploeg, Martine van der (2023). *Future drought and groundwater availability in the Netherlands: a growing concern*. Tech. rep. Accessed: 03.01.2025. Copernicus Meetings. URL: https://meetingorganizer.copernicus.org/GC8-Hydro/GC8-Hydro-88.html.

Berghuijs, Wouter R., Hale, Kate, Beria, Harsh (2025). "Streamflow Seasonality using Directional Statistics". In: *EGUsphere* 2025, pp. 1–16. DOI: https://doi.org/10.5194/egusphere-2024-4117.

Bollen, Matthijs (2025). "Controls on rainfall-recharge dynamics in England". MA thesis. Free University Amsterdam.

Bosveld, Fred C. (2020). "The Cabauw in-situ observational program 2000–present: Instruments, calibrations and set-up". In: *History* 19, pp. 8–6. URL: https://cdn.knmi.nl/knmi/pdf/bibliotheek/knmipubTR/TR384.pdf.

Boumis, Georgios, Kumar, Mukesh, Nimmo, John R., Clement, T. Prabhakar (2022). "Influence of Shallow Groundwater Evapotranspiration on Recharge Estimation Using the Water Table Fluctuation Method". In: *Water Resources Research* 58. DOI: https://doi.org/10.1029/2022WR032073.

Brauer, Claudia (2014). *Data description document for groundwater level measurements Cabauw Experimental Site for Atmospheric Research (CESAR)*. Accessed: 04.01.2025. URL: https://ruisdael-observatory.nl/cesar-database/pages/datasetsKDC.html.

Brauer, Claudia, Torfs, PJJF., Teuling, AJ., Uijlenhoet, R. (2014). "The Wageningen Lowland Runoff Simulator (WALRUS): Application To The Hupsel Brook Catchment And The Cabauw Polder". In: *Hydrology and Earth System Sciences* 18.10, pp. 4007–4028. DOI: https://doi.org/10.5194/hess-18-4007-2014.

Bresser, A. H. M., Berk, M. M., Born, G. J. van den, Bree, L. van, Galen, E. W. van, Ligtvoet, W., Minnen, J. G. van, Witmer, M. C. H. (2005). *The effect of climate change in the Netherlands. Report number: 773001037*. Tech. rep. Netherlands Environmental Assesment Agency. URL: https://www.pbl.nl/sites/default/files/downloads/773001037.pdf.

Cao, Guoliang, Scanlon, Bridget R., Han, Dongmei, Zheng, Chunmiao (2016). "Impacts of thickening unsaturated zone on groundwater recharge in the North China Plain". In: *Journal of hydrology* 537, pp. 260–270. DOI: https://doi.org/10.1016/j.jhydrol.2016.03.049.

Chang, Yin-Lung, Tsai, Tung-Lin, Yang, Jinn-Chuang (2019). "Flood hazard mitigation in land subsidence prone coastal areas by optimal groundwater pumping". In: *Journal of Flood Risk Management* 12.S2, e12517. DOI: https://doi.org/10.1111/jfr3.12517.

Cheng, Yanyan, Ogden, Fred L., Zhu, Jianting (2017). "Earthworms and tree roots: A model study of the effect of preferential flow paths on runoff generation and groundwater recharge in steep, saprolitic, tropical lowland catchments". In: *Water Resources Research* 53.7, pp. 5400–5419. URL: https://agupubs.onlinelibrary.wiley.com/doi/full/10.1002/2016WR020258.

Collenteur, Raoul A., Bakker, Mark, Caljé, Ruben, Klop, Stijn A., Schaars, Frans (2019). "Pastas: open source software for the analysis of groundwater time series". In: *Groundwater* 57.6, pp. 877–885. DOI: https://doi.org/10.1111/gwat.12925.

Collenteur, Raoul A., Bakker, Mark, Klammler, Gernot, Birk, Steffen (2021). "Estimation of groundwater recharge from groundwater levels using nonlinear transfer function noise models and comparison to lysimeter data". In: *Hydrology and Earth System Sciences* 25.5, pp. 2931–2949. DOI: https://doi.org/10.5194/hess-25-2931-2021.

Cook, Peter G., Walker, Glen Russell (1990). *The effect of soil type on groundwater recharge in the Mallee region. Report no. 28*. Centre for Groundwater Studies.

Crosbie, Russell S., Binning, Philip, Kalma, Jetse D. (2005). "A time series approach to inferring groundwater recharge using the water table fluctuation method". In: *Water Resources Research* 41.1. DOI: https://doi.org/10.1029/2004WR003077.

Crosbie, Russell S., Doble, Rebecca C., Turnadge, Chris, Taylor, Andrew R. (2019). "Constraining the magnitude and uncertainty of specific yield for use in the water table fluctuation method of estimating recharge". In: *Water Resources Research* 55.8, pp. 7343–7361. DOI: https://doi.org/10.1029/2019WR025285.

Cuthbert, Mark O., Taylor, Richard G., Favreau, Guillaume, Todd, Martin C., Shamsudduha, Mohammad, Villholth, Karen G., MacDonald, Alan M., Scanlon, Bridget R., Kotchoni, DO Valerie, Vouillamoz, Jean-Michel, et al. (2019). "Observed controls on resilience of groundwater to climate variability in sub-Saharan Africa". In: *Nature* 572.7768, pp. 230–234. DOI: https://doi.org/10.1038/s41586-019-1441-7.

Cuthbert, MO. (2010). "An improved time series approach for estimating groundwater recharge from groundwater level fluctuations". In: *Water Resources Research* 46.9. DOI: https://doi.org/10.1029/2009WR008572.

Cuthbert, MO., Nimmo, JR. (2013). "Linking soil moisture balance and source-responsive models to estimate diffuse and preferential components of groundwater recharge". In: *Hydrology and Earth System Sciences* 17.3, pp. 1003–1019. DOI: https://doi.org/10.5194/hess-17-1003-2013.

De Beek, CZ. van, Leijnse, H., Torfs, PJJF., Uijlenhoet, R. (2011). "Climatology of daily rainfall semivariance in The Netherlands". In: *Hydrology and earth system sciences* 15.1, pp. 171–183. DOI: https://doi.org/10.5194/hess-15-171-2011.

De Vries, Jacobus J. (2007). "Groundwater". In: *Geology of the Netherlands*. Ed. by TE. Wong, DAJ. Batjes, J. de Jager, Koninklijke Nederlandse Akademie van Wetenschappen. Royal Netherlands Academy of Arts and Sciences. URL: https://www.researchgate.net/publication/46686954_Geology_of_the_Netherlands.

De Vries, Jacobus J., Simmers, Ian (2002). "Groundwater recharge: an overview of processes and challenges". In: *Hydrogeology journal* 10, pp. 5–17. DOI: https://doi.org/10.1007/s10040-001-0171-7.

Delin, Geoffrey N., Healy, Richard W., Lorenz, David L., Nimmo, John R. (2007). "Comparison of local- to regional-scale estimates of ground-water recharge in Minnesota, USA." In: *Journal of Hydrology* 334.1-2, pp. 231–249. DOI: https://doi.org/10.1016/j.jhydrol.2006.10.010.

Dingman, S Lawrence (2015). *Physical hydrology*. Waveland press. ISBN: 978-1-4786-1118-9.

DINOloket (2022). *Data and information on the Dutch subsurface*. Accessed: 04.05.2025. URL: https://www.dinoloket.nl/en/subsurface-data.

Doble, Rebecca C., Crosbie, Russell S. (2017). "Current and emerging methods for catchment-scale modelling of recharge and evapotranspiration from shallow groundwater". In: *Hydrogeology journal* 25.1, p. 3. DOI: https://doi.org/10.1007/s10040-016-1470-3.

Dripps, WR. (2012). "An integrated field assessment of groundwater recharge". In: *Open Hydrology Journal* 6, pp. 15–22. DOI: https://doi.org/10.2174/1874378101206010015.

Eaton, Timothy T. (2020). "Episodic and continuous recharge estimation from high-resolution well records". In: *Groundwater* 58.4, pp. 511–523. DOI: https://doi.org/10.1111/gwat.12950.

Eden, Jonathan M., Kew, Sarah F., Bellprat, Omar, Lenderink, Geert, Manola, Iris, Omrani, Hiba, Oldenborgh, Geert Jan van (2018). "Extreme precipitation in the Netherlands: An event attribution case study". In: *Weather and climate extremes* 21, pp. 90–101. DOI: https://doi.org/10.1016/j.wace.2018.07.003.

Engelenburg, Jolijn van, Hueting, Rosa, Rijpkema, Sjoerd, Teuling, Adriaan J., Uijlenhoet, Remko, Ludwig, Fulco (2018). "Impact of changes in groundwater extractions and climate change on groundwater-dependent ecosystems in a complex hydrogeological setting". In: *Water resources management* 32, pp. 259–272. DOI: https://doi.org/10.1007/s11269-017-1808-1.

Eslami, Zahra, Seybold, Hansjörg, Kirchner, James W. (2025). "Climatic, topographic, and groundwater controls on runoff response to precipitation: evidence from a large-sample data set". In: *EGUsphere* 2025, pp. 1–15. DOI: https://doi.org/10.5194/egusphere-2025-35.

Farmer, Darren, Sivapalan, Murugesu, Jothityangkoon, Chatchai (2003). "Climate, soil, and vegetation controls upon the variability of water balance in temperate and semiarid landscapes: Downward approach to water balance analysis". In: *Water Resources Research* 39.2. DOI: https://doi.org/10.1029/2001WR000328.

Free University Amsterdam (n.d.). *Generative AI., Copilot and ChatGPT*. Continuously updated. Accessed: 07.10.2024 and 26.06.2025. URL: https://vu.nl/en/student/examinations/generative-ai-your-use-our-expectations.

Freyberg, Jana von, Moeck, Christian, Schirmer, Mario (2015). "Estimation of groundwater recharge and drought severity with varying model complexity". In: *Journal of Hydrology* 527, pp. 844–857. DOI: https://doi.org/10.1016/j.jhydrol.2015.05.025.

Gao, Huibin, Ju, Qin, Zhang, Dawei, Wang, Zhenlong, Hao, Zhenchun, Kirchner, James W. (2025a). "Quantifying dynamic linkages between precipitation, groundwater recharge, and streamflow using ensemble rainfall-runoff analysis". In: *Water Resources Research* 61.1, e2024WR037821. DOI: https://doi.org/10.1029/2024WR037821.

Gao, Huibin, Pfister, Laurent, Kirchner, James W. (2025b). "Quantifying controls on rapid and delayed runoff response in double-peak hydrographs using Ensemble Rainfall-Runoff Analysis (ERRA)". In: *EGUsphere* 2025, pp. 1–32. DOI: https://doi.org/10.5194/egusphere-2025-613.

Genuchten, M Th van (1980). "A closed-form equation for predicting the hydraulic conductivity of unsaturated soils". In: *Soil science society of America journal* 44.5, pp. 892–898.

Gorkum, Max van (2025). "A comparison of observed and modelled precipitation-streamflow relationships in two Dutch catchments using Ensemble Rainfall-Runoff Analysis (ERRA)". MA thesis. Free University Amsterdam.

Griebler, Christian, Avramov, Maria (2015). "Groundwater ecosystem services: a review". In: *Freshwater Science* 34.1, pp. 355–367. DOI: https://doi.org/10.1086/679903.

Grillakis, Manolis G. (2019). "Increase in severe and extreme soil moisture droughts for Europe under climate change". In: *Science of the Total Environment* 660, pp. 1245–1255. DOI: https://doi.org/10.1016/j.scitotenv.2019.01.001.

Guillaumot, Luca, Longuevergne, Laurent, Marçais, Jean, Lavenant, Nicolas, Bour, Olivier (2022). "Frequency domain water table fluctuations reveal impacts of intense rainfall and vadose zone thickness on groundwater recharge". In: *Hydrology and Earth System Sciences* 26.22, pp. 5697–5720. DOI: https://doi.org/10.5194/hess-26-5697-2022.

Gumula-Kawecka, Anna, Jaworska-Szulc, Beata, Szymkiewicz, Adam, Gorczewska-Langner, Wioletta, Pruszkowska-Caceres, Malgorzata, Angulo-Jaramillo, Rafael, Simunek, Jirka (2022). "Estimation of groundwater recharge in a shallow sandy aquifer using unsaturated zone modeling and water table fluctuation method". In: *Journal of Hydrology* 605, p. 127283. DOI: https://doi.org/10.1016/j.jhydrol.2021.127283.

Healy, Richard W. (2010). *Estimating groundwater recharge*. Cambridge university press. DOI: https://doi.org/10.1017/CBO9780511780745.

Healy, Richard W., Cook, Peter G. (2002). "Using groundwater levels to estimate recharge". In: *Hydrogeology journal* 10, pp. 91–109. DOI: https://doi.org/10.1007/s10040-001-0178-0.

Hendriks, DMD., Kuijper, MJM., Ek, R. van (2014). "Groundwater impact on environmental flow needs of streams in sandy catchments in the Netherlands". In: *Hydrological Sciences Journal* 59.3-4, pp. 562–577. DOI: https://doi.org/10.1080/02626667.2014.892601.

Heppner, Christopher S., Nimmo, John R. (2005). *A computer program for predicting recharge with a master recession curve*. US Geological Survey Menlo Park, CA., USA. URL: http://pubsdata.usgs.gov/pubs/sir/2005/5172/.

Hocking, Mark, Kelly, Bryce FJ. (2016). "Groundwater recharge and time lag measurement through Vertosols using impulse response functions". In: *Journal of Hydrology* 535, pp. 22–35. DOI: https://doi.org/10.1016/j.jhydrol.2016.01.042.

Hosseinzadehtalaei, Parisa, Tabari, Hossein, Willems, Patrick (2020). "Climate change impact on short-duration extreme precipitation and intensity–duration–frequency curves over Europe". In: *Journal of Hydrology* 590, p. 125249. DOI: https://doi.org/10.1016/j.jhydrol.2020.125249.

Huang, Yanan, Evaristo, Jaivime, Li, Zhi (2019). "Multiple tracers reveal different groundwater recharge mechanisms in deep loess deposits". In: *Geoderma* 353, pp. 204–212. DOI: https://doi.org/10.1016/j.geoderma.2019.06.041.

Huijgevoort, Marjolein HJ. van, Voortman, Bernard R., Rijpkema, Sjoerd, Nijhuis, Kelly HS., Witte, Jan-Philip M. (2020). "Influence of climate and land use change on the groundwater system of the Veluwe, The Netherlands: A historical and future perspective". In: *Water* 12.10, p. 2866. DOI: https://doi.org/10.3390/w12102866.

Hund, Silja V., Allen, Diana M., Morillas, Laura, Johnson, Mark S. (2018). "Groundwater recharge indicator as tool for decision makers to increase socio-hydrological resilience to seasonal drought". In: *Journal of Hydrology* 563, pp. 1119–1134. DOI: https://doi.org/10.1016/j.jhydrol.2018.05.069.

Hunt, R.andall J., Prudic, David E., Walker, John F., Anderson, Mary P. (2008). "Importance of unsaturated zone flow for simulating recharge in a humid climate". In: *Groundwater* 46.4, pp. 551–560. DOI: https://doi.org/10.1111/j.1745-6584.2007.00427.x.

Hurk, Bart van den, Siegmund, Peter, Klein Tank, Albert, Attema, Jisk, Bakker, Alexander, Beersma, Jules, Bessembinder, Janette, Boers, Reinout, Brandsma, Theo, Brink, Henk van den, Drijfhout, Sybren, Eskes, Henk, Haarsma, Rein, et al. (2014). "KNMI'14: Climate Change scenarios for the 21st Century–A Netherlands perspective". In: *KNMI: De Bilt, The Netherlands*. URL: https://www.knmiprojects.nl/binaries/knmiprojects/documenten/publications/2014/05/26/knmi-wr-2014-01/KNMI_WR_2014-01_version26May2014.pdf.

Jasechko, Scott, Birks, S Jean, Gleeson, Tom, Wada, Yoshihide, Fawcett, Peter J., Sharp, Zachary D., McDonnell, Jeffrey J., Welker, Jeffrey M. (2014). "The pronounced seasonality of global groundwater recharge". In: *Water Resources Research* 50.11, pp. 8845–8867. DOI: https://doi.org/10.1002/2014WR015809.

Jasechko, Scott, Taylor, Richard G. (2015). "Intensive rainfall recharges tropical groundwaters". In: *Environmental Research Letters* 10.12, p. 124015. DOI: https://doi.org/10.1088/1748-9326/10/12/124015.

Jasechko, Scott, Wassenaar, Leonard I., Mayer, Bernhard (2017). "Isotopic evidence for widespread cold-season-biased groundwater recharge and young streamflow across central Canada". In: *Hydrological Processes* 31.12, pp. 2196–2209. DOI: https://doi.org/10.1002/hyp.11175.

Jie, Zhang, Heyden, Jan van, Bendel, David, Barthel, Roland (2011). "Combination of soil-water balance models and water-table fluctuation methods for evaluation and improvement of groundwater recharge calculations". In: *Hydrogeology Journal* 19.8, p. 1487. URL: https://link.springer.com/article/10.1007/s10040-011-0772-8.

Joustra, D., Jalink, M., Dorland, E., Huijskes, H., H., Lantink, Oling, A., J.W., Jansen (2017). *PAS-gebiedsanalyse 060 Stelkampsveld*. Accessed 21.05.2025. URL: https://www.natura2000.nl/sites/default/files/PAS/Gebiedsanalyses_vigerend/060_Stelkampsveld_gebiedsanalyse_15-12-17_GL.pdf.

Kim, John H., Jackson, Robert B. (2012). "A global analysis of groundwater recharge for vegetation, climate, and soils". In: *Vadose Zone Journal* 11.1, vzj2011–0021RA. DOI: https://doi.org/10.2136/vzj2011.0021RA.

Kirchner, James W. (2022). "Impulse response functions for nonlinear, nonstationary, and heterogeneous systems, estimated by deconvolution and demixing of noisy time series". In: *Sensors* 22.9, p. 3291. DOI: https://doi.org/10.3390/s22093291.

— (2024). "Characterizing nonlinear, nonstationary, and heterogeneous hydrologic behavior using ensemble rainfall–runoff analysis (ERRA): proof of concept". In: *Hydrology and Earth System Sciences* 28.19, pp. 4427–4454. DOI: https://doi.org/10.5194/hess-28-4427-2024.

— (2025). *An introduction to ERRA*. Accessed: 09.06.2025. URL: https://www.envidat.ch/dataset/erra-an-r-script-for-ensemble-rainfall-runoff-analysis/resource/0c048816-816a-4c1f-bedf-32be20e4d4c2?inner_span=True.

Kishel, Hans F., Gerla, Philip J. (2002). "Characteristics of preferential flow and groundwater discharge to Shingobee Lake, Minnesota, USA." In: *Hydrological Processes* 16.10, pp. 1921–1934. DOI: https://doi.org/10.1002/hyp.363.

Koirala, Sujan, Kim, Hyungjun, Hirabayashi, Yukiko, Kanae, Shinjiro, Oki, Taikan (2019). "Sensitivity of global hydrological simulations to groundwater capillary flux parameterizations". In: *Water Resources Research* 55.1, pp. 402–425. DOI: https://doi.org/10.1029/2018WR023434.

Kumar, Raaghul, Yazdan, Munshi Md Shafwat (2022). "Evaluating Preventive Measures for Flooding from Groundwater: A Case Study". In: *J.* 6.1, pp. 1–16. DOI: https://doi.org/10.3390/j6010001.

Labrecque, Geneviève, Chesnaux, Romain, Boucher, Marie-Amélie (2020). "Water-table fluctuation method for assessing aquifer recharge: application to Canadian aquifers and comparison with other methods". In: *Hydrogeology Journal* 28.2, pp. 521–533. DOI: https://doi.org/10.1007/s10040-019-02073-1.

Lai, Xiaoming, Liao, Kaihua, Feng, Huihui, Zhu, Qing (2016). "Responses of soil water percolation to dynamic interactions among rainfall, antecedent moisture and season in a forest site". In: *Journal of Hydrology* 540, pp. 565–573. DOI: https://doi.org/10.1016/j.jhydrol.2016.06.038.

Leerdam, RC. van, Rook, JH., Riemer, L., Aa, NGFM. van der (2023). "Waterbeschikbaarheid voor de bereiding van drinkwater tot 2030-knelpunten en oplossingsrichtingen". In: *RIVM rapport 2023-0005*. Rijksinstituut voor Volksgezondheid en Milieu RIVM. URL: http://www.rivm.nl/bibliotheek/rapporten/2023-0005.pdf.

Leth, Thomas C. van, Leijnse, Hidde, Overeem, Aart, Uijlenhoet, Remko (2021). "Rainfall spatiotemporal correlation and intermittency structure from micro-γ to meso-β scale in the Netherlands". In: *Journal of Hydrometeorology* 22.8, pp. 2227–2240. DOI: https://doi.org/10.1175/JHM-D-20-0311.1.

Levintal, Elad, Kniffin, Maribeth L., Ganot, Yonatan, Marwaha, Nisha, Murphy, Nicholas P., Dahlke, Helen E. (2023). "Agricultural managed aquifer recharge (Ag-MAR)—a method for sustainable groundwater management: A review". In: *Critical Reviews in Environmental Science and Technology* 53.3, pp. 291–314. DOI: https://doi.org/10.1080/10643389.2022.2050160.

Li, Zhi, Chen, Xi, Liu, Wenzhao, Si, Bingcheng (2017). "Determination of groundwater recharge mechanism in the deep loessial unsaturated zone by environmental tracers". In: *Science of the Total Environment* 586, pp. 827–835. DOI: https://doi.org/10.1016/j.scitotenv.2017.02.061.

Liu, Xiuhua, Gao, W.ande, Sun, Shijun, Hu, Anyan, He, Yi, He, ShuaiShuai (2019). "Responses of soil water dynamic processes and groundwater recharge to irrigation intensity and antecedent moisture

in the vadose zone". In: *Hydrological processes* 33.5, pp. 849–863. DOI: https://doi.org/10.1002/hyp.13368.

Lizard Viewer (2025). *Groundwater stations*. Accessed: 23.04.2025. URL: https://vitens.lizard.net/viewer/map.

Long, Andrew J. (2015). "RRAWFLOW: Rainfall-response aquifer and watershed flow model (v1. 15)". In: *Geoscientific Model Development* 8.3, pp. 865–880. DOI: https://doi.org/10.5194/gmd-8-865-2015.

Mann, Henry B., Whitney, Donald R. (1947). "On a test of whether one of two random variables is stochastically larger than the other". In: *The annals of mathematical statistics*, pp. 50–60. DOI: https://doi.org/10.1214/aoms/1177730491.

MAQ Observations - Data Downloads) (2025). *Veenkampen: Meteorology and Soil*. Accessed: 23.04.2025. URL: https://maq-observations.nl/data-downloads/.

Mathias, Simon, Sorensen, James, Butler, Adrian (2017). "Soil moisture data as a constraint for groundwater recharge estimation". In: *Journal of Hydrology* 552, pp. 258–266. DOI: https://doi.org/10.1016/j.jhydrol.2017.06.040.

Meteorology and Air Quality Group, University of Wageningen (2018). *Veenkampen*. Accessed: 08.02.2025. URL: https://maq-observations.nl/veenkampen/.

Moeck, Christian, Brunner, Philip, Hunkeler, Daniel (2016). "The influence of model structure on groundwater recharge rates in climate-change impact studies". In: *Hydrogeology Journal* 24.5, p. 1171. DOI: https://doi.org/10.1007/s10040-016-1367-1.

Moeck, Christian, Grech-Cumbo, Nicolas, Podgorski, Joel, Bretzler, Anja, Gurdak, Jason J., Berg, Michael, Schirmer, Mario (2020). "A global-scale dataset of direct natural groundwater recharge rates: A review of variables, processes and relationships". In: *Science of the total environment* 717, p. 137042. DOI: https://doi.org/10.1016/j.scitotenv.2020.137042.

Moeck, Christian, Radny, Dirk, Popp, Andrea, Brennwald, Matthias, Stoll, Sebastian, Auckenthaler, Adrian, Berg, Michael, Schirmer, Mario (2017). "Characterization of a managed aquifer recharge system using multiple tracers". In: *Science of the Total Environment* 609, pp. 701–714. URL: https://doi.org/10.1016/j.scitotenv.2017.07.211.

Naeimi, Golnar (2021). "Assessment of drought impacts on groundwater table in the Netherlands using gridded datasets in Google Earth Engine (GEE)". MA thesis. University of Twente. URL: http://essay.utwente.nl/89004/.

O'driscoll, MA., DeWalle, DR., McGuire, KJ., Gburek, WJ. (2005). "Seasonal 18O variations and groundwater recharge for three landscape types in central Pennsylvania, USA." In: *Journal of Hydrology* 303.1-4, pp. 108–124. DOI: https://doi.org/10.1016/j.jhydrol.2004.08.020.

OpenStreetMap (2024). Accessed: 08.12.2024. URL: https://www.openstreetmap.org.

Owuor, Steven O., Butterbach-Bahl, Klaus, Guzha, Alphonce Chenjerayi, Rufino, Mariana C., Pelster, David E., Díaz-Pinés, Eugenio, Breuer, Lutz (2016). "Groundwater recharge rates and surface runoff response to land use and land cover changes in semi-arid environments". In: *Ecological Processes* 5, pp. 1–21. DOI: https://doi.org/10.1186/s13717-016-0060-6.

P.andas Community (2008). *pandas.DataFrame.diff documentation*. Continuously updated. Accessed: 09.02.2025. URL: https://pandas.pydata.org/docs/reference/api/pandas.DataFrame.diff.html.

— (2025). *pandas.DataFrame.resample documentation*. Continuously updated. Accessed: 17.05.2025. URL: https://pandas.pydata.org/pandas-docs/stable/reference/api/pandas.DataFrame.resample.html.

Peterson, TJ., Western, AW. (2014). "Nonlinear time-series modeling of unconfined groundwater head". In: *Water Resources Research* 50.10, pp. 8330–8355. DOI: https://doi.org/10.1002/2013WR014800.

Puntu, Jordi Mahardika, Chang, Ping-Yu, Amania, Haiyina Hasbia, Lin, Ding-Jiun, Sung, Chia-Yu, Suryantara, M Syahdan Akbar, Chang, Liang-Cheng, Doyoro, Yonatan Garkebo (2023). "Groundwater monitoring and specific yield estimation using time-lapse electrical resistivity imaging and

machine learning". In: *Frontiers in Environmental Science* 11, p. 1197888. DOI: https://doi.org/10.3389/fenvs.2023.1197888.

Royal Netherland Meteorological Institute (KNMI) (2025a). *cesar_soil_water_lb1_t10*. Accessed: 23.04.2025. URL: https://dataplatform.knmi.nl/dataset/cesar-soil-water-lb1-t10-v1-1.

— (2025b). *cesar_surface_meteo_lc1_t10*. Accessed: 23.04.2025. URL: https://dataplatform.knmi.nl/dataset/cesar-surface-meteo-lc1-t10-v1-0.

— (2025c). *Uurgegevens van het weer in Nederland*. Accessed 07.03.2025. URL: https://www.knmi.nl/nederland-nu/klimatologie/uurgegevens.

— (n.d.). Accessed: 10.06.2025. URL: https://www.knmi.nl/klimaat-viewer/kaarten/neerslag-verdamping/gemiddelde-hoeveelheid-neerslagoverschot/jaar/Periode_1981-2010.

Ruisdael Observatory (2018a). *Cabauw*. Accessed: 20.12.2024. URL: https://ruisdael-observatory.nl/cabauw/.

— (2018b). *Veenkampen*. Accessed: 08.02.2025. URL: https://ruisdael-observatory.nl/veenkampen/.

Salem, Ali, Abduljaleel, Yasir, Dezső, József, Lóczy, Dénes (2023). "Integrated assessment of the impact of land use changes on groundwater recharge and groundwater level in the Drava floodplain, Hungary". In: *Scientific Reports* 13.1, p. 5061. DOI: https://doi.org/10.1038/s41598-022-21259-4.

Scanlon, Bridget R., Healy, Richard W., Cook, Peter G. (2002). "Choosing appropriate techniques for quantifying groundwater recharge". In: *Hydrogeology journal* 10, pp. 18–39. URL: https://link.springer.com/article/10.1007/s10040-001-0176-2.

Scipy Community (2008a). *scipy.optimize.curve_fit documentation*. Continuously updated. Accessed: 12.03.2025. URL: https://docs.scipy.org/doc/scipy/reference/generated/scipy.optimize.curve_fit.html.

— (2008b). *scipy.stats.spearmanr*. Continuously updated. Accessed: 08.04.2025. URL: https://docs.scipy.org/doc/scipy/reference/generated/scipy.stats.spearmanr.html.

— (2008c). *Statistical functions (scipy.stats): mannwhitneyu*. Accessed: 18.04.2025. URL: https://docs.scipy.org/doc/scipy/reference/generated/scipy.stats.mannwhitneyu.html.

Singh, Ajay, P.anda, Sudhindra N., Uzokwe, Veronica NE., Krause, Peter (2019). "An assessment of groundwater recharge estimation techniques for sustainable resource management". In: *Groundwater for Sustainable Development* 9, p. 100218. DOI: https://doi.org/10.1016/j.gsd.2019.100218.

Siyuan, Huo, Menggui, Jin, Liang, Xing, Li, Xiang, Hongbo, Hao (2020). "Estimating impacts of water-table depth on groundwater evaporation and recharge using lysimeter measurement data and bromide tracer". In: *Hydrogeology Journal* 28.3, pp. 955–971. DOI: https://doi.org/10.1007/s10040-019-02098-6.

Smerdon, BD., Mendoza, CA., Devito, KJ. (2008). "Influence of subhumid climate and water table depth on groundwater recharge in shallow outwash aquifers". In: *Water Resources Research* 44.8. DOI: https://doi.org/10.1029/2007WR005950.

Sobaga, Antoine, Habets, Florence, Beaudoin, Nicolas, Léonard, Joël, Decharme, Bertrand (2024). "Decreasing trend of groundwater recharge with limited impact of intense precipitation: Evidence from long-term lysimeter data". In: *Journal of Hydrology* 637, p. 131340. DOI: https://doi.org/10.1016/j.jhydrol.2024.131340.

Spannenberg, Jescica, Atangana, Abdon, Vermeulen, PD. (2017). "New non-linear model of groundwater recharge: Inclusion of memory, heterogeneity and visco-elasticity". In: *Open Geosciences* 9.1, pp. 436–441. DOI: https://doi.org/10.1515/geo-2017-0033.

Szilagyi, Jozsef, Zlotnik, Vitaly A., Jozsa, Janos (2013). "Net recharge vs. depth to groundwater relationship in the Platte River Valley of Nebraska, United States". In: *Groundwater* 51.6, pp. 945–951. DOI: https://doi.org/10.1111/gwat.12007.

Tashie, Arik M., Mirus, Benjamin B., Pavelsky, Tamlin M. (2016). "Identifying long-term empirical relationships between storm characteristics and episodic groundwater recharge". In: *Water Resources Research* 52.1, pp. 21–35. DOI: https://doi.org/10.1002/2015WR017876.

Teo, Chuan Jiet, Poinapen, Johann, Hofman, JAMH., Wintgens, Thomas (2025). "Assessing water dependencies and risks in Dutch industries: Distribution, consumption and future challenges". In: *Water Resources and Industry* 33, p. 100279. DOI: https://doi.org/10.1016/j.wri.2025.100279.

Thissen, Wil, Kwakkel, Jan, Mens, Marjolein, Sluijs, Jeroen van der, Stemberger, Sara, Wardekker, Arjan, Wildschut, Diana (2017). "Dealing with uncertainties in fresh water supply: Experiences in the Netherlands". In: *Water resources management* 31, pp. 703–725. DOI: https://doi.org/10.1007/s11269-015-1198-1.

Turkeltaub, T., Kurtzman, D., Bel, G., Dahan, O. (2015). "Examination of groundwater recharge with a calibrated/validated flow model of the deep vadose zone". In: *Journal of Hydrology* 522, pp. 618–627. DOI: https://doi.org/10.1016/j.jhydrol.2015.01.026.

Velde, Rogier van der (2022). *Twelve years profile soil moisture and temperature measurements in Twente, the Netherlands*. Version V2. DOI: 10.17026/dans-znj-wyg5. URL: https://doi.org/10.17026/dans-znj-wyg5.

Vonk, Martin (2021). "Performance of nonlinear time series models to simulate synthetic groundwater table time series from an unsaturated zone model". MA thesis. Delft University of Technology. URL: https://repository.tudelft.nl/record/uuid:36191e86-d81e-464f-94ab-b573d95c99ab#files.

Wageningen Environmental Research (2024). *L.andelijk grondgebruik Nederland*. Accessed: 12.12.2024. URL: https://lgn.nl/bestanden.

— (2025). *Imminent drought in The Netherlands: groundwater levels plummet due to dry spring*. Accessed: 01.05.2025. URL: https://www.wur.nl/en/research-results/research-institutes/environmental-research/show-wenr/imminent-drought-in-the-netherlands-groundwater-levels-plummet-due-to-dry-spring-1.htm.

Wageningen University (2025). *cesar_groundwater_levelhourly_la1_t1h_v1.0*. Accessed: 23.04.2025. URL: https://dataplatform.knmi.nl/dataset/cesar-grndwater-level-la1-t1h-v1-0.

Walczuk, André, Campos, José Eloi Guimarães, Teles, Lucas Santos Batista (2025). "Potential and effective recharge of the Federal District shallow aquifers, Brazilian savanna region-coupled analysis of GLDAS-2, Water Table Fluctuation (WTF) and rainfall pattern". In: *Journal of South American Earth Sciences*, p. 105426. DOI: https://doi.org/10.1016/j.jsames.2025.105426.

Walker, David, Parkin, Geoff, Schmitter, Petra, Gowing, John, Tilahun, Seifu A., Haile, Alemseged T., Yimam, Abdu Y. (2019). "Insights from a multi-method recharge estimation comparison study". In: *Groundwater* 57.2, pp. 245–258. DOI: https://doi.org/10.1111/gwat.12801.

Wang, Xihua, Zhang, Guangxin, Xu, Y Jun (2014). "Spatiotemporal groundwater recharge estimation for the largest rice production region in Sanjiang Plain, Northeast China". In: *Journal of Water Supply: Research and Technology—AQUA*. 63.8, pp. 630–641. DOI: https://doi.org/10.2166/aqua.2014.024.

Waterschap Rijn end IJssel (2024). *Leidingvak, Watergang*. Accessed 28.12.2024. URL: https://opendata-wrij.opendata.arcgis.com/.

— (2025). *Webapp Meetlocaties Hydrologie*. Accessed 28.04.2025. URL: https://wrij.maps.arcgis.com/apps/webappviewer/index.html?id=bdf79c0c783a4825a086ae023d222f12.

Wendt, Doris Elise, Loon, Anne F. van, Scanlon, Bridget R., Hannah, David M. (2021). "Managed aquifer recharge as a drought mitigation strategy in heavily-stressed aquifers". In: *Environmental Research Letters* 16.1, p. 014046. DOI: https://doi.org/10.1088/1748-9326/abcfe1.

Wiel, Karin van der, Beersma, Jules, Brink, Henk van den, Krikken, Folmer, Selten, Frank, Severijns, Camiel, Sterl, Andreas, Meijgaard, Erik van, Reerink, Thomas, Dorland, Rob van (2024). "KNMI'23 climate scenarios for the Netherlands: storyline scenarios of regional climate change". In: *Earth's Future* 12.2, e2023EF003983. DOI: https://doi.org/10.1029/2023EF003983.

Wilopo, Wahyu, Putra, Doni Prakasa Eka (2021). "Groundwater recharge estimation using groundwater level fluctuation patterns in unconfined aquifer of Yogyakarta City, Indonesia". In: *Kuwait Journal of Science* 48.2. DOI: https://doi.org/10.48129/kjs.v48i2.9397.

Witte, Jan-Philip M., Runhaar, J., Ek, R. van (2009). *Ecohydrologische effecten van klimaatverandering op de vegetatie van Nederland*. KWR. URL: https://edepot.wur.nl/143420.

Witte, Jan-Philip M., Zaadnoordijk, Willem Jan, Buyse, Jan Jaap (2019). "Forensic hydrology reveals why groundwater tables in the province of Noord Brabant (the Netherlands) dropped more than expected". In: *Water* 11.3, p. 478. DOI: https://doi.org/10.3390/w11030478.

Xie, Yueqing, Crosbie, Russell, Yang, Jie, Wu, Jichun, Wang, Wenke (2018). "Usefulness of soil moisture and actual evapotranspiration data for constraining potential groundwater recharge in semiarid regions". In: *Water Resources Research* 54.7, pp. 4929–4945. DOI: https://doi.org/10.1029/2018WR023257.

Yang, Chunliu, Wu, Jianhua, Li, Peiyue, Wang, Yuanhang, Yang, Ningning (2023). "Evaluation of soil-water characteristic curves for different textural soils using fractal analysis". In: *Water* 15.4, p. 772. DOI: https://doi.org/10.3390/w15040772.

Zaadnoordijk, W., Lourens, A. (2019). "Groundwater dynamics in the aquifers of the Netherlands". In: *TNO report. TNO 2019 R12031*. URL: https://www.grondwatertools.nl/sites/default/files/2023-07/ZaadnoordijkLourens2019_GroundwaterDynamicsInTheAquifersOfTheNetherlands_TNO-R12031.pdf.

Zaadnoordijk, Willem, Bus, Stefanie, Lourens, Aris, Berendrecht, Wilbert L. (2019). "Automated time series modeling for piezometers in the national database of the Netherlands". In: *Groundwater* 57.6, pp. 834–843. DOI: https://doi.org/10.1111/gwat.12819.

Zhang, Jien, Felzer, Benjamin S., Troy, Tara J. (2016). "Extreme precipitation drives groundwater recharge: The northern high plains aquifer, central United States, 1950–2010". In: *Hydrological Processes* 30.14, pp. 2533–2545. DOI: https://doi.org/10.1002/hyp.10809.